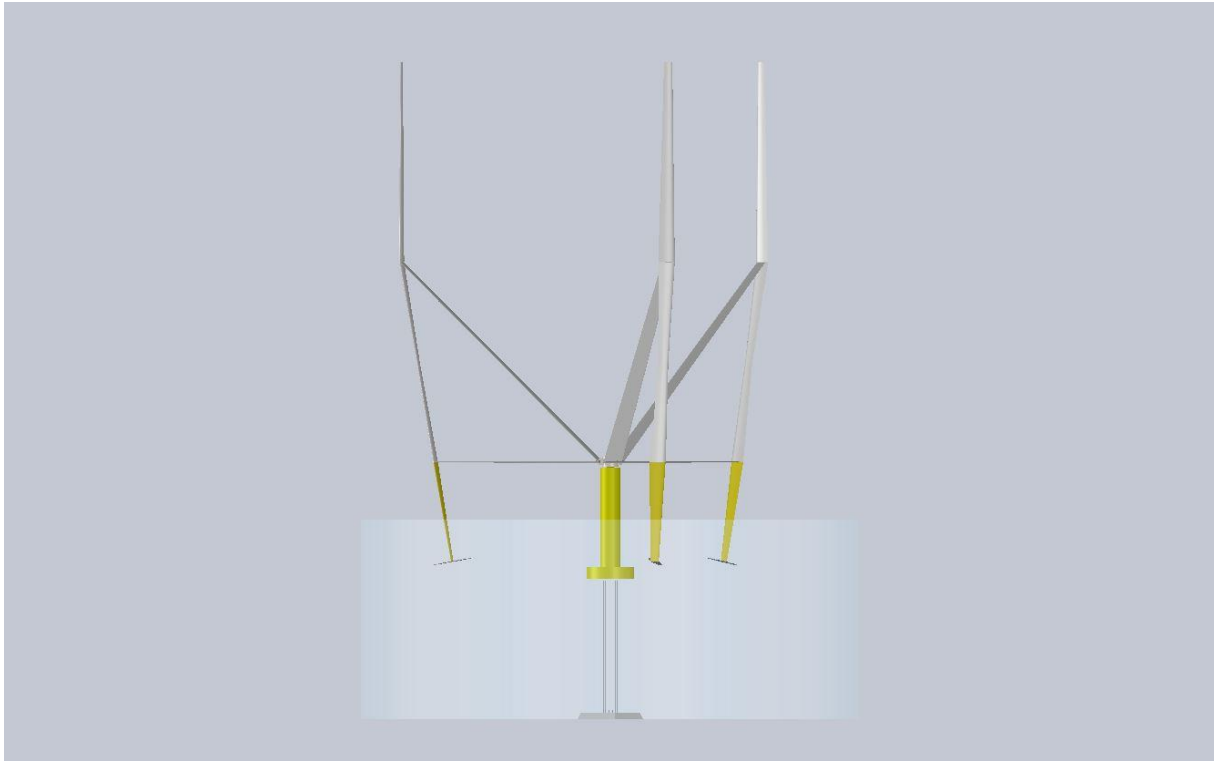


VERTICAL AXIS OFFSHORE WIND TURBINE



KJETIL VIKEN
TORE TOTLAND SKJERDAL

Bachelor's thesis in Energy Technology
Bergen, Norway 2020

VERTICAL AXIS OFFSHORE WIND TURBINE

Kjetil Viken
Tore Totland Skjerdal

Department of Mechanical- and Marine Engineering
Western Norway University of Applied Sciences
NO-5063 Bergen, Norway

Høgskulen på Vestlandet
Fakultet for Ingeniør- og Naturvitskap
Institutt for maskin- og marinfag
Inndalsveien 28
NO-5063 Bergen, Norge

Cover image © MantaWind

Backside image © ROC CANALS PHOTOGRAPHY/GETTY IMAGES

Norsk tittel: Vertikal akslet offshore vindturbin

Author(s), student number: Kjetil Viken h572005
Tore Totland Skjerdal h182721

Study program: Energy technology
Date: May 2020
Report number: IMM 2020-M72
Supervisor at HVL: Jan Michael Simon Bartl
Assigned by: Western Norway University of Applied Sciences

Antall filer levert digitalt: 10/10

Preface

This bachelor thesis is written for Western Norway University of Applied Sciences, at the Department of Mechanical and Marine Engineering, campus Bergen. Our internal supervisor is Jan Michael Simon Bartl and our external supervisor is Ph.D. Magnus Rahm, the CEO of Manta Wind AB.

We wish to thank Bernt Hustad Hemre, for designing and assembling the load cell used in the thesis. We would also like to thank Jan Michael Simon Bartl and Ph.D. Magnus Rahm for their support on writing the thesis, giving us academical and professional input.

Abstract

The world is undergoing a change from a high-carbon community to a low-carbon community, where the need for renewable energy is high. This increases the need for offshore wind turbines. A low weight offshore wind turbine is favorable to a high weight offshore wind turbine, due to desired benefits as lower maintenance, lower construction cost, less materials used, etc. Manta Wind's concept is based upon a low weight vertical axis wind turbine, leading to a decreased levelized cost of energy.

This rapport investigates the use of different wingtip configurations, and a turbine-wing interaction on the underwater hydrofoils connected to Manta Wind's turbine-concept. The scientific investigations were done both theoretically and experimentally. The theoretical method was based upon excel-calculations based on lift and drag values from Xfoil, while the experimental method focused on hydrodynamic resistance tests in a tow-tank, at Western Norway University of Applied Sciences with lift and drag measurements by a load cell.

The theoretical test shows what forces we can expect to find on a full-scale manta wind turbine, as well as which dimension the underwater hydrofoil needs to have to be able to lift the whole construction at start-up velocity. When comparing the experimental values with the theoretical values, for the prototype tested, the result differs due to factors as stall and limitations in the theoretical calculations. A comparison of different wingtips shows a small difference in lift - and drag coefficients. Showing that the design of a winglet/wingtip influences lift and drag over a hydrofoil. A small comparison of the effect of Reynolds number shows how little it influences the forces working on a hydrofoil. When testing the underwater hydrofoil and looking at the effect of a disc-wing interaction a clear difference in lift and drag can be spotted. With the drag-disc giving the hydrofoil a higher drag coefficient and lower lift coefficient. Finally, the experiment shows that the winglet with the highest angle from the vertical axis gives the best lift-to-drag ratio, and combined with a drag-disc, giving us the desired output of lift and drag.

Sammendrag

Verden gjennomgår en endring fra et høg-karbon samfunn til et lav-karbon samfunn, der behovet for fornybar energi er stort. Dette øker behovet for offshore vindmøller. En offshore vindmølle med lav vekt er gunstig i forhold til en vindmølle med høy vekt på grunn av ønskede fordeler som lavere vedlikehold, lavere byggekostnad, mindre materialer brukt etc. Manta Winds konsept er basert på en vertikal akse vindmølle med lav vekt, noe som fører til redusert energikostnad. Denne rapporten undersøker bruken av forskjellige vingetuppkonfigurasjoner, og en turbin-vinge-interaksjon på en undervanns hydrofoil som skal være koblet til Manta Winds turbinkonsept. De vitenskapelige undersøkelsene ble gjort både teoretisk og eksperimentelt. Den teoretiske metoden er basert på Excel-beregninger basert på lift- og drag verdier fra Xfoil, mens den eksperimentelle metoden fokuserer på hydrodynamiske motstandsforsøk i en slepetank, ved Høgskolen på Vestlandet, med lift- og drag målinger ved bruk av en lastcelle.

Den teoretiske testen viser hvilke krefter som kan forventes på en fullskala Manta-vindturbin, samt hvilken dimensjon undervannshydrofoilen trenger for å kunne løfte hele konstruksjonen ved oppstarthastighet. Når man sammenligner de eksperimentelle verdiene med de teoretiske verdiene, for prototypen som er testet, skiller resultatet seg ut på grunn av faktorer som stall og begrensninger i de teoretiske beregningene. En sammenligning av forskjellige vingetupper viser en liten forskjell i lift- og drag koeffisienter. Noe som viser at utformingen av en vinge / vingetupp påvirker lift og drag over en hydrofoil. En liten sammenligning av effekten av Reynolds-tallet viser hvor lite det påvirker kreftene som virker på en hydrofoil. Når du tester hydrofoilen under vann og ser på effekten av et samspill mellom disken og vingen, kan man oppdage en tydelig forskjell i lift og drag. Med drag disken gir hydrofoilen en høyere drag koeffisient og lavere løfte koeffisient. Til slutt viser eksperimentet at wingleten med den største vinkelen fra den vertikale aksen gir det beste forholdet mellom lift og drag. Denne i kombinasjon med drag disken gir oss det beste utfallet av lift og drag.

Table of Contents

Preface.....	V
Abstract	VII
Sammendrag.....	IX
1. Introduction	1
2. Theory	3
2.1 Vertical-Axis-Wind turbine.....	3
2.1.1 Manta Wind concept	6
2.2 Hydrofoil	6
2.2.1 Hydrofoil theory	8
2.2.2 Turbulent and laminar flow	9
2.2.3 NACA0012.....	11
2.3 Winglet design.....	12
2.4 Actuator disc.....	14
2.4.1 Theory	15
2.4.2 Interaction disc – hydrofoil	15
2.5 Scale-modelling.....	17
2.5.1 Froude Number.....	17
2.5.2 Reynolds Number.....	18
3. Experimental method	19
3.1 MarinLab.....	19
3.2 Load Cells	20
3.2.1 Strain gauges	20
3.2.2 Dimensioning of the load cells.....	20
3.2.3 Load Cell Calibration	22
3.3 Wingtips	22
3.4 Force measurements.....	23
3.5 Test matrix explanation.....	25
3.6 Potential error sources	25
3.7 Lab procedure.....	26

3.7.1	Assemble hydrofoil	26
3.7.2	Calibrate load cells	26
3.7.3	Connecting to tow-wagon.....	27
3.7.4	Testing.....	27
3.7.5	Deviation in angle of attack.....	28
3.8	Reynolds number in the tow-tank	28
4.	Theoretical method.....	29
4.1	Geometric design and data	29
4.1.1	Assumptions and demands	29
4.1.2	Steps	30
4.1.3	Calculations	30
4.2	Calculations of angle of attack	31
5.	Result.....	32
5.1	Theoretical result on the full-scale wing section.....	32
5.1.1	Manta Wind dimensions, based upon start-up velocity.....	34
5.2	Experimental results on the model-scale wing section.....	35
5.2.1	Lift and Drag force timeseries.....	35
5.2.2	Comparison Experiment vs theory	36
5.2.3	Comparison of wingtip configurations	37
5.2.4	Effect of Reynolds number.....	39
5.2.5	Effect of disc-wing interaction	40
6.	Conclusion.....	41
7.	References	42
8.	Table of figures	44
9.	Table of Equations.....	46
10.	Table of tables	46
	Attachments.....	47

1. Introduction

Offshore wind energy and renewable energy are in focus like never before. Several large companies, such as Equinor and Aker Solution, are investing heavily in developing new technology to make offshore wind farms more attractive and profitable. With projects such as the Hywind and the Windfloat-concept, one can see that there is a great willingness to seek new solutions to improve the technology within floating wind turbines. Most of the major projects in progress are based on large floating horizontal-axis wind turbines, HAWT. These wind turbines are massive structures that extend high above sea level. This entails large investments in material, which is pushing the levelized cost of energy, LCOE, up. Due to huge investments and new technology LCOE is expected to drop for floating offshore wind. [1] One of the contributors is the Swedish company MantaWind, which was started by Magnus Rahm. They aim to reduce the weight of an offshore wind turbine by 70 per cent, and thereby reduce LCOE by 50 per cent, thus making offshore wind more economical [2]. By using a vertical axis topology, VAWT, one gets added benefits of the design on the rest of the system. Buoyancy and stability are the main particulars of a floating wind turbine. This is solved by what is the key behind the weight reduction of the turbine. Higher accelerations can be achieved by removing both tower and nacelle. As shown in Figure 1-1, we see how the wind turbine is designed, where a VAWT with three blades, in combination with underwater wings and turbines, will contribute to lower weight and increased LCOE.

In this assignment, the focus will be on the effect of different wingtip configurations, on an underwater hydrofoil, and how these affect lift and drag. The main objective of this hydrofoil is to lift the vertical wind turbine blades above the water line. There will be tested variations of wingtips, velocities and angle of attack. Different analysis and tests will be done in MarinLab at the Western Norway University of Applied Science in Bergen, with a prototype sent from Manta Wind. The lift and drag forces, which work on the underwater wing, will be investigated using load cells. Combination of different wingtips will be tested to see how they will affect lift- and drag coefficient. The underwater wing itself is of the type NACA0012, as shown in Figure 1-2, and consists of both a vertical and horizontal part. The turbine is tested using an actuator disk.

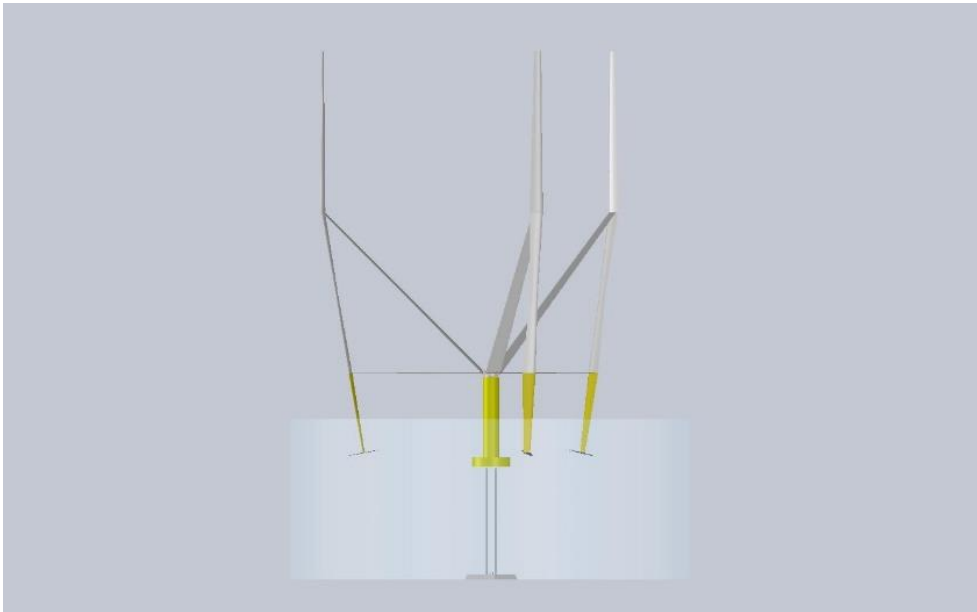


Figure 1-1, Manta Wind ABS prototype



Figure 1-2, NACA0012 prototype hydrofoil

2. Theory

2.1 Vertical-Axis-Wind turbine

Wind turbines designs are divided into two main categories, Horizontal axis wind turbine, HAWT, and Vertical axis wind turbine, VAWT. The most commonly used wind turbine is the HAWT design, but there are several ongoing projects on the VAWT design, done by several individual developers. [3] Even though VAWT is not used in big-industrial-scale wind energy production today, it has some advantages. The turbines generator and gearbox can be placed closed to the ground, which will result in easier maintenance and lower construction costs. A problem with the VAWT design is that the turbine is located closer to the ground where the windspeed is lower, which will affect the magnitude of effect that can be extracted from the wind. VAWT is mainly divided into two different designs, the Savonius rotor and the Darreius model. Savonius wind turbine is a slow rotating, high torque machine which normally have two or more scoops. Mostly it is used in high-reliability low-efficiency turbines. Opposite from other turbines the Savonius don't use lift generated by airfoil-shaped blades to drive a rotor, it uses drag and therefore can't rotate faster than the approaching wind speed. [4] This is the most popular of the two types because it does not need an external power source to start up.



Figure 2-1. Savonius-Rotor [5]

The Darriues wind turbine is also known as an Eggbeater turbine and was invented by Georges Darreius in 1931. His design has a vertical shaft supporting two thin, curved aerofoil blades, each in the shape of a bow, with the ends of each blade attached to the top and bottom in the shaft. [6] It is a high speed, low torque machine suitable for generating alternating current (AC) electricity.

[4] Starting torque on this turbine is very low, therefore an external power source is needed to the start up. The design of this turbine makes it great at efficiency, however they are not very reliable.



Figure 2-2. Experimental Department of energy (DOE) and US Department of Agriculture (USDA) 34-meter diameter Darrieus Wind turbine [7]

Another configuration, also patented by Darrieus, is the H-shaped rotor in which the blades of the rotor are vertical but straight so the whole rotor has the shape of a capital H. This type of rotor is called a Giromill. [8] Early designs for the H-configuration was originally proposed and developed by Peter Musgrove in 70's, 80's and 90's. The development of this configuration went through a succession of succeeding larger turbines in England. [9] According to Wilson analysis of a Giromill, an H-type turbine with cyclically pitching blades has the same limit as a HAWT, which is the Betz limit. [10]



Figure 2-3, H-rotor design [7]

VAWT is sometimes loosely categorized as lift- and drag-based design. With design from the nature the blades move perpendicular at the wind direction. Due to this factor the turbine is able to utilize the wind from every direction. Unlike the HAWT, which uses the yaw-gear to turn the turbine in the right direction to utilize the wind. A disadvantage with the VAWT Darrieus-turbine is that the blades usual is twice as long as a HAWT. At the other side the blades are attached to the center of the tower in both ends, which does that they are mainly loaded with tensions and can be made lighter than a HAWT. [9]

The VAWT's position has worsened the last years due to missing development in the last two decades, even though its design has a significantly advantages when it comes to offshore applications. One big advantage is that the unit can be placed on or under the water surface, while one of the biggest disadvantages is the long blades and a missing reliable aerodynamic brake-system which cannot use pitch-regulation as an alternative solution. [9]

2.1.1 Manta Wind concept

Manta Winds concept is most similar to the H-shaped rotor. The vertical axis topology is used due to the added benefits it gives in design of the rest of the system. The main particulars of a floating wind turbine are buoyancy and stability, which is solved in an entirely new way. It can persist higher accelerations because of the lack of both a tower and a nacelle. [2] The hub of the rotor is located on top of deck of the buoyancy column and the rotor blades attached to the hub by a hinge point. The point is to reduce the LCOE by 50% and the weight by 70%.

The Manta Wind turbine is held up by three underwater hydrofoils, which main purpose is to lift the construction up above the waterline, once the start-up velocity is reached. This start-up velocity is at 3,5m/s. On each of this hydrofoil, a turbine is located. Once the wind turbine is in flight mode, meaning that the construction has lifted its wings above the waterline and started to spin, power extraction happens on each of the underwater turbines. Transforming the kinetic energy in the water to electric energy. Meaning that the vertical axis rotor blades of the wind turbine uses the wind to rotate the underwater hydrofoils, and thus extracting energy.

2.2 Hydrofoil

In this experiment an underwater wing, also called hydrofoil, is used to lift the vertical wind turbine blades above the waterline. Hydrofoils have the same main principles as airfoils, which has been used in the aircraft industry for many years, with the only difference being the fluid in which they operate in. The use of airfoils is extremely central in the aerospace industry and is utilized to create lift so that aircraft can manage to lift off the ground. When a single hydrofoil is parallel to the velocity of a moving

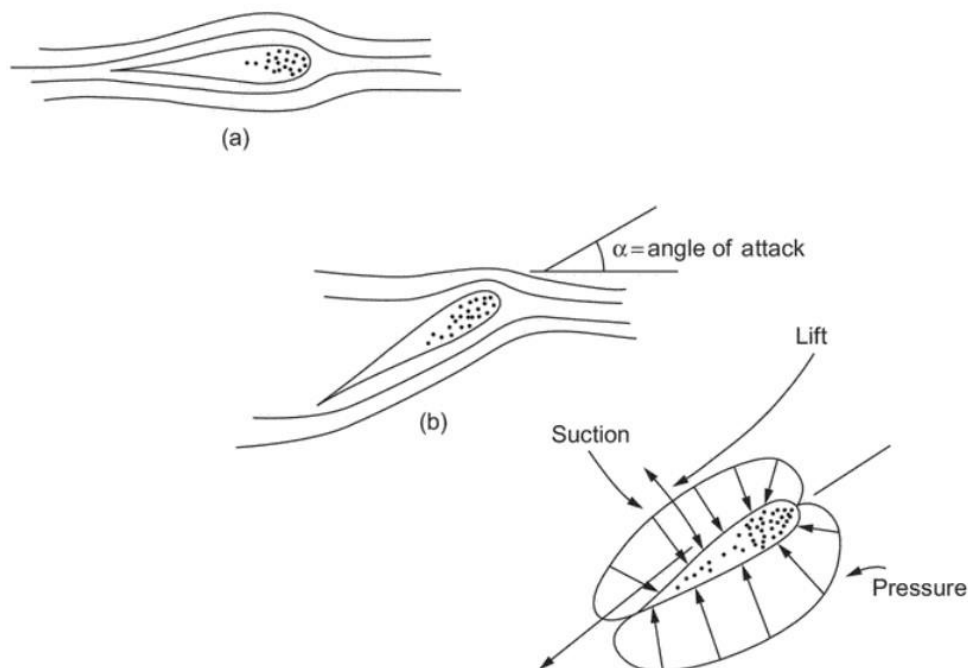


Figure 2-4, How a Fluid flows around a hydrofoil

fluid, the fluid-flow will divide around the body of the hydrofoil by separating at the leading edge and reassemble at the trailing edge. The main fluid-stream will not experience any permanent deflections due to the wing. Forces are applied to the foil by the local distribution of the fluid and the friction of the fluid on the surface. If the hydrofoil has an increased angle of attack against the fluid-stream, then there will be a greater disturbance on the stream and the streamline pattern will change. The fluid undergoes a local deflection, although the fluid-flow is still parallel and uniform a distance in front of and behind the hydrofoil.

As shown in Figure 2-4b, the upstream disturbance will be much less than the downstream disturbance. According to Newton's laws, the local deflection of the fluid-stream can only be achieved if the wing exerts a force on the fluid, thus forcing the fluid to react by producing an equal and opposite force on the hydrofoil. The foil, by being present in the stream, changes the local pressure distribution and the local velocities, which can be explained by Bernoulli's equation. By examination of the streamlines around the hydrofoil in Figure 2-4b, one can see that the streamlines over the hydrofoil approaches each other, indicating an increase in speed and a reduction in static pressure. While below the hydrofoil, the angle of attack on the wing will separate the streamlines, which will result in an increase in static pressure. [11]

Measurements of pressure at various points on the surface of the hydrofoil will show a pressure distribution as shown in Figure 2-4c. The vectorial sum of these pressures will produce a resultant force acting on the hydrofoil. This resultant force can decompose into a lift component L and a drag component D . The resultant force is assumed to act through a definite point located in the hydrofoil, so that the behavior of the force will be the same as if all the individual components acted simultaneously. It is possible to measure lift and drag forces for all values of fluid-stream velocity, angle of attack and various airfoil types. By using such observed values one can define the relationship between the forces:

$$C_D = \frac{D}{\frac{1}{2}A\rho V^2}$$

Equation 1, Lift Coefficient

$$C_L = \frac{L}{\frac{1}{2}A\rho V^2}$$

Equation 2, Drag Coefficient

Where

C_L = Lift coefficient

C_D = Drag coefficient

L= Lift force

D= Drag force

A= Surface area

ρ = Fluid density

V= Fluid velocity

The biggest difference between flow in water and air is the density and the fact that water is incompressible and that it is possible to experience cavitation. [11]

2.2.1 Hydrofoil theory

Wind turbine blades are long and narrow structures where the velocity component in the wingspan direction is much lower than in the flow direction, and it is therefore assumed in many aerodynamic models that the streamflow at a given radial position is two-dimensional and that 2-D airfoil data can be used. A two-dimensional stream consists of a plane and if this plane is described as shown in Figure 2-5 then the velocity component in the Z-direction will be equal to zero.

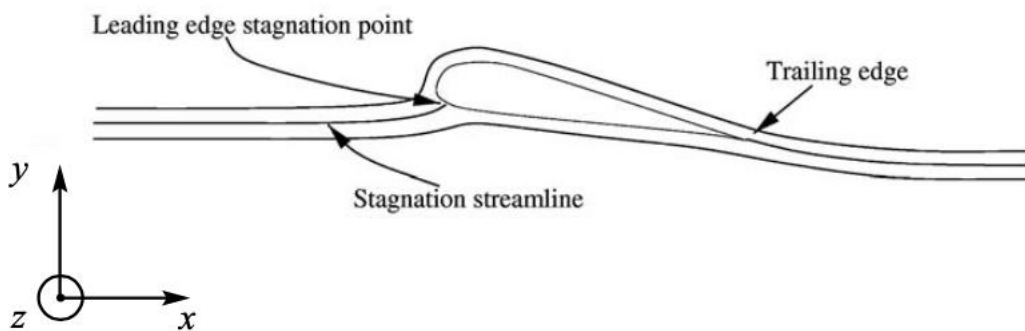


Figure 2-5, Schematic view of streamlines past a hydrofoil

Figure 2-5 shows the leading stagnation point in a two-dimensional stream past an airfoil. The reacting force F from the fluid flow is decomposed to a direction perpendicular to the velocity at infinite V_∞ , Lift, and to a direction parallel to V_∞ , Drag. This definition of lift and drag can be seen in Figure 2-6.

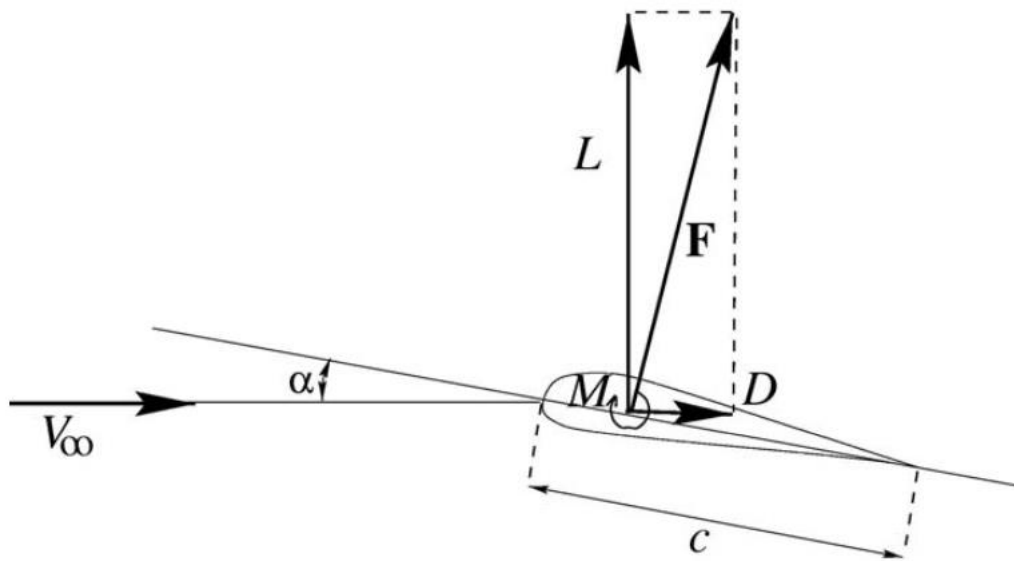


Figure 2-6, Definition of lift and drag

If the airfoil is designed for an aircraft, it is relevant that the lift to drag ratio is maximized. To be able to lift a mass from the ground, the lift force must overcome the gravitational force and the higher the lift force the greater mass can lift from the ground. The same concept is important for Manta Wind's turbine. The lift-forces is needed to lift the construction up from the water surface and into flight-mode, which is explained in chapter 2.1.1

The physical explanation for lift is that the shape of the hydrofoil forces the streamlines to curve around the geometry, as indicated in Figure 2-4. It is known from basic fluid mechanics that the pressure gradient, $\frac{\partial p}{\partial r} = \frac{\rho V^2}{r}$, is required to curve the streamlines. Where r is the curvature of the streamlines and V is the velocity. This pressure gradient acts as a centrifugal force, known from the circular motion of a particle. Since there is atmospheric pressure far from the hydrofoil, it must have a pressure lower than the atmospheric pressure on the top of the foil and a higher pressure on the underside of the foil. It is this pressure difference that creates the lift force on the hydrofoil. [12]

2.2.2 Turbulent and laminar flow

The type of flow streaming around the hydrofoil can affect the lift and drag forces working on the hydrofoil. In a turbulent stream, the velocity of the fluid is at a point that continuously undergoes changes in both magnitude and direction. The air or water swirls and eddies while its overall bulk of fluid moves along in a specific direction. Most types of fluid flows are turbulent, except laminar flows at the leading edge of, for example, a hydrofoil [13]. In comparison, a laminar flow is a fluid that moves smoothly or in regular patterns. In a laminar flow, the velocity, pressure, and other fluid properties of

the fluid are constant at each point. [14] The transition from laminar to turbulent flow does not occur suddenly; rather, it occurs over some region in which the flow fluctuates between laminar and turbulent flows before it becomes fully turbulent. Wherever the flow is laminar or turbulent is linked to Reynolds number, which can be calculated from the velocity of the fluid, the chord length of a hydrofoil and kinematic viscosity of a fluid.

2.2.2.1 Boundary layer

In 1904 Ludwig Prandtl made a breakthrough in fluid mechanics and introduced the boundary layer approximation. The idea behind this approximation is to divide the flow into two regions; an outer flow region, which is inviscid and/or irrotational, and inner flow region, called the boundary layer. The boundary layer is a very thin region of flow near a solid wall where viscous forces and rotationality cannot be ignored. [15] The boundary layer is the layer of fluid from the surface of the hydrofoil to the point where there is no measurable fluid velocity. We have two types of boundary layer flows: laminar and turbulent.

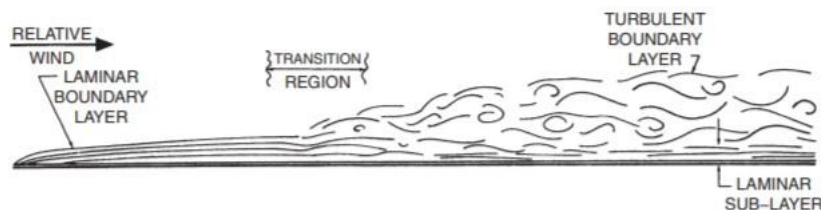


Figure 2-7. Boundary layer composition

Boundary layers in stagnation regions and in rapidly accelerating flows, such found at the forward regions of a hydrofoil, are relatively stable to disturbance. A reasonable assumption is that the flow over the leading edge of the wing is laminar and makes the transition to fully turbulent flow at a fixed distance from the leading edge.

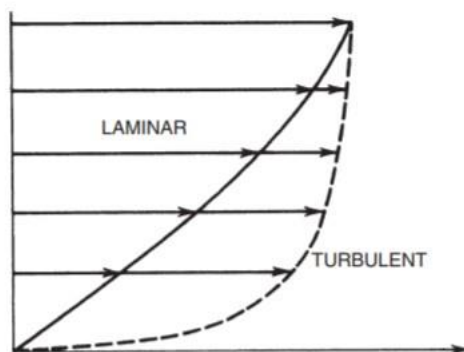


Figure 2-8. Boundary layer velocity profile

As shown in Figure 2-8 velocity profiles are different in laminar and turbulent flows. Where laminar profiles show a gradual decrease in the relative velocity from the outer edge of the boundary layer to the surface, turbulent flow involves rapid intermixing of the air levels, and faster moving air speeds up

the particles near the surface. [16] Given that a laminar boundary layer has substantially lower drag, it would often be recommended trying to increase the laminar extent. [17] [18]

2.2.3 NACA0012

NACA is a method for indicating various characteristics of a hydrofoil/airfoil. Different types of NACA airfoils, meaning National Advisory Committee for Aeronautics, are identified through different number codes.

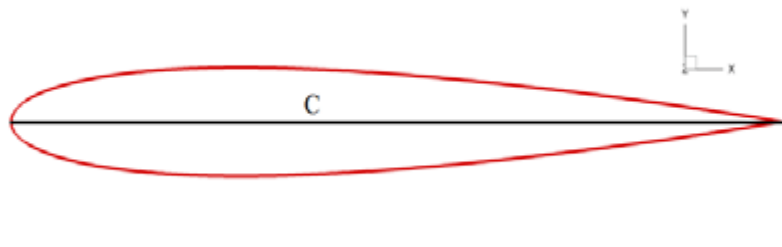


Figure 2-9. NACA0012 profile

In a NACA 4-digit airfoil, the first number explains the camber as a percentage of the chord, the second number gives the location of the maximum camber point in the tenths of a chord, and the last two digits give the thickness as a percentage of the arc.

Meaning that the NACA0012 Hydrofoil has the given characteristics:

- Max camber 0% at 0% chord
- Max thickness 12% at 30% chord.

[19]

Different NACA-profiles has different lift- and drag coefficients, depending on the fluid moving around the foil, Reynolds number and turbulence. These coefficients can be found on pages like airfoiltools.com.

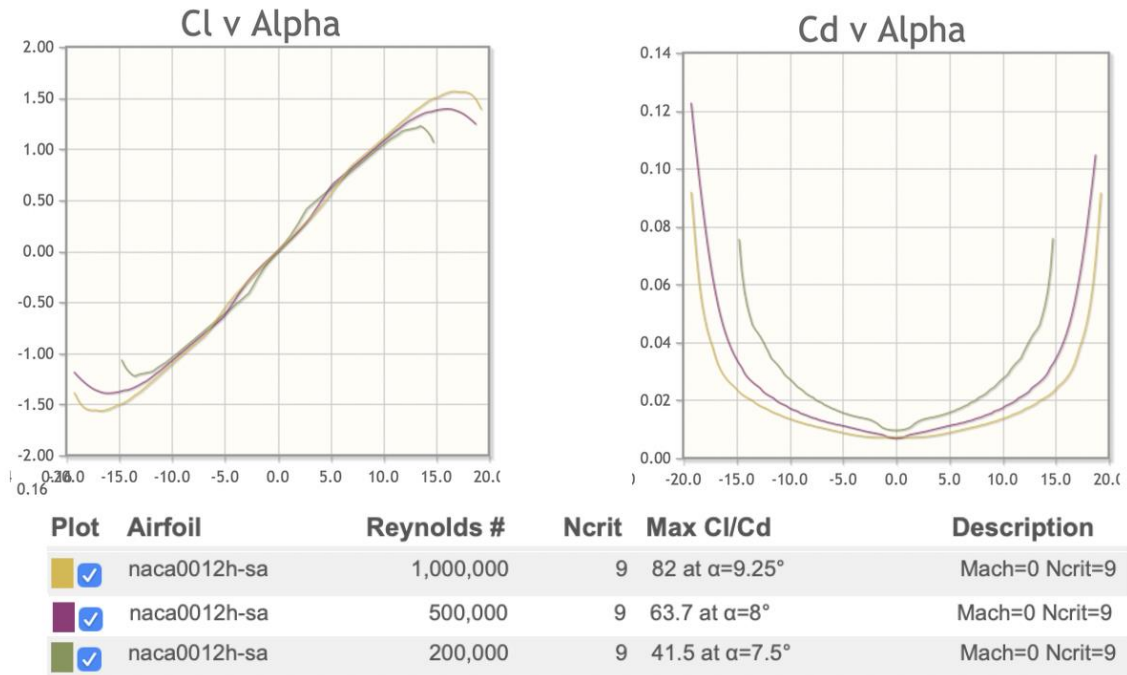


Figure 2-10, Different graphs of a NACA0012 hydrofoil. Re number ranging between 200.00 and 500.000

The graphs shown in Figure 2-10 is calculated by the *website airfoiltools* by using a program called Xfoil, created by Mark Drela and Harold Youngren for the design and analysis of subsonic airfoils, where the Ncrit value is used to model the turbulence of the fluid. A Ncrit value of 9 equals the turbulence of an average wind tunnel, while a Ncrit value between 4-8 equals a dirty wind tunnel. [20]

2.3 Winglet design

Winglets have been used since the start of 20th century. These small tips are designed to increase the efficiency of the plane and to reduce the drag force. The inspiration behind winglets comes from nature itself. Many birds curl their wingtips upwards to increase the efficiency of their flight. This is especially normal for birds who uses their wings to glide, which is



Figure 2-12, Winglet Design on a glider plane



Figure 2-11, Inspiration behind a winglet comes from nature

the same concept planes use. [21] The reason behind the use of winglets is to reduce the vortices-drag, which is high during take-off and landing. Wingtip vortices reduce the effective lift-creating wing surface, and winglets are mostly installed to reduce the fuel consumption and minimize drag. Vortices are created on the wingtips when air, with high pressure, changes to low-pressure air during take-off and landing. The occurrence of drag will then occur because the vortices has lower pressure than the air passing over the wing.

There are many different kinds of winglets and their purpose is the same, but the design is different. Winglets influence the design of the plane, which is the main reason they are not similar. The most common types of winglets are: squared, rounded, floppy-tips, and mixed winglets where they bend upward gradually from the wing at approximately 70 degrees angel. Some planes are designed with raked wingtips, which reduces the fuel consumption, increase lift properties and reduces the take-off length.

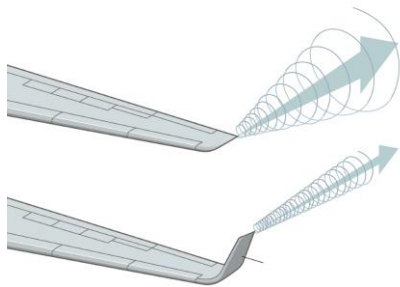


Figure 2-13, How the winglet affects the airstream

Not every plane is designed with winglets. Advantage due to reduced fuel consumption needs to be big enough to counter the extra weight which the winglets add. An easier way to improve the efficiency is to increase the length of the wingspan. But this requires a bigger area for the plane to land on and will not be a good solution for planes who must land on smaller airports. These planes would rather benefit from the use of winglets.

The induced drag of a wing with limited span already exists in a not viscous flow. It is generally assumed that the viscosity of the flow does not affect the induced drag, and its therefore seen as non-existent or disappearing. A not-viscous flow can't develop vortices, it must continue to be a potential flow as it was on an earlier point. An example of this is that a parallel flow with constant velocity remains a potential flow even though you add a solid body. [22]

Flow around the lifting wings cannot be explained without lifting vortices bounded to the wing. Vortices cannot end in the flow, they continue in a vortex wake, which represent a singularity in the wake. At all other points, the flow is potential. Vortices at variable strength cannot exist without other vortices affecting it.

Lifting Line theory

The lifting line theory was developed by Ludwig Prandtl in 1918. This theory is used to calculate the lift-distribution of the wingspan. In this theory the vortices are assumed to be parallel to the non-distributed flow vector velocity-infinity. The theory can be problematic when the wing has a dihedral

angle, which is an angle from the wing to the horizontal plane. Forces due to the lifting vortices induces on it itself becomes infinity, which becomes a positive induced lift upwards and a negative induced lift downward where the opposite is true. [23]

Drag and lift

There are many factors which influence the amount of aerodynamic drag which the body generates. Drag depends on the shape, size and inclination of the object, and flow conditions of the air passing it [24]. Winglets affect the induced drag, which the magnitude is determined by the spanwise distribution of vortices shed downstream of the wing trailing edge, which is related in turn to the spanwise lift distribution. Induced drag can, as mentioned before, be reduced by increasing the span and by increasing the vertical height of the lifting system. [25] Flow around the wingtips have a strong influence on the induced drag or drag due to lift, which its often called. This is because of the vortices which is created there. Several attempts have been done to reduce the induced drag by shaping winglets and wingtips. Flight test at NASA Dryden Flight Research Center have found a 6,5% reduction in fuel use of a Boeing 707 type airliner when using winglets. Winglets must be carefully integrated into the total wing design, which, as mentioned before, is one of the main reasons there are many different types of winglets.

2.4 Actuator disc

An actuator disc is used to analyze the aerodynamic behavior of wind turbines by replacing the swept area of a wind turbine with a surface force that act upon the incoming flow. The actuator disc is also used to analyze how wake effect can affect the streamflow behind a turbine. As can be seen in Figure 2-14, an actuator disc will affect the behavior of a fluid flow. The actuator disc is a vertically porous flat plate with an area S which encounters a non-compressible fluid with a density of ρ moving at a uniform speed U .

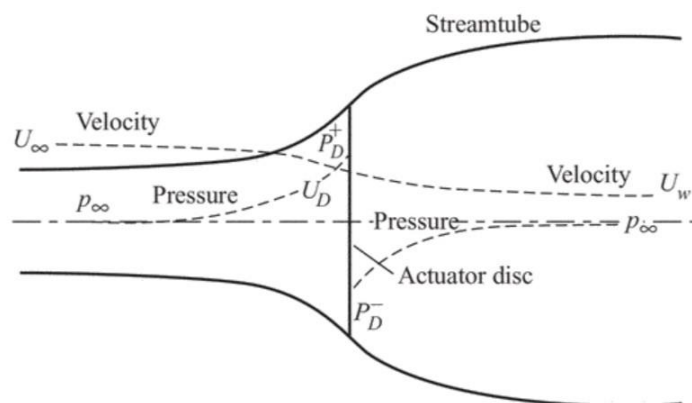


Figure 2-14. Actuator disc

2.4.1 Theory

The simple axial-moment theory originates from Rankine, W. Froude and R.E. Froude, and it is this theory the actuator disk is based on. [26]

The actuator disc momentum theory is often used to mathematically describe the energy extraction process and how the kinetic energy is extracted. The three conservation laws, mass, energy and momentum, are applied to a flow inside a stream tube where a fluid is passing through the disc. By looking at Figure 2-14, one can see that the cross-sectional area is smaller upstream of the disk than downstream. The expansion of the stream tube is due to the fact that the mass flow velocity must be equal everywhere. The mass of the fluid, air or water, that are passing through a given cross-sectional area of the stream tube for a given period of time, is ρAU , where ρ is the air density, A is the cross-sectional area and U is the stream rate. Since the velocity of mass flow must be equal over the entire stream tube the following formula is given by:

$$\rho A_{\infty} U_{\infty} = \rho A_D U_D = \rho A_W U_W$$

Equation 3, Mass flow velocity

The symbol ∞ refers to conditions far upstream, D refers to conditions at the actuator disk and W refers to conditions far behind the disk in the wake effect that occurs. It is common to assume that the actuator disc induces a velocity variation that must be imposed over the free stream rate.

[27]

2.4.2 Interaction disc – hydrofoil

The interaction between an actuator disc and a hydrofoil can somehow be compared to a propeller/wing interaction on an aircraft. By taking into account that the airframe interaction with the propeller slipstream is important for the propeller location optimization. This interaction between propeller and wing will affect the aircraft's performance, and as well be important for cruise conditions, transonic flight speed and moderate thrust, and take-off cases, low speed and high thrust. [28] But it is important to keep in mind that a water turbine (actuator disc) extracts energy from the flow while a ship or aircraft propeller adds energy to the flow.

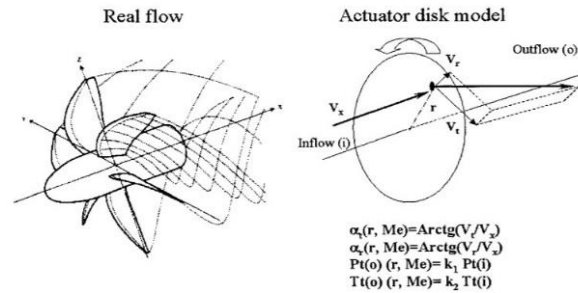


Figure 2-15, Rotating flow behind a turbine VS the flow behind an actuator disc

The interaction between an actuator disc and a hydrofoil can be analyzed by looking at the flow around the object. A drag disc gives no rotating wake and the flow through and around the disc will become symmetrical. The wake from a drag disc will give completely different inflow conditions on the hydrofoil compared to if there is no drag disc. It is also important to notice that there will also be a big difference between a drag disc and a rotating turbine rotor.

If the water turbine rotor (Drag Disc) is placed behind the hydrofoil, the inflow to the hydrofoil will instead be affected by the inflow velocity, in an area upstream of the water turbine, being lower with lower lift and drag as a result. The total lift force from the hydrofoil will thus decrease compared to when there is no turbine at all.

As mentioned in *Aerodynamic effect of wingtip-mounted propellers and turbines*, it has been suggested that large propulsive efficiency benefits and significant induced drag reductions can be achieved if turbines are mounted at the wingtips. The benefits of this involve both that large amount of energy/power can be generated with little drag penalty and that in some cases power extraction results in a net drag reduction. The paper concludes with it being some significant potential performance benefits like reduction in the power required to maintain a given flight condition, translating into a reduction of drag forces working on the wing. [29]

To completely understand how the flow will interact with the actuator disc and the airfoil it is important to understand how Betz's Law works and how the flow of water looks like in a wake. Betz's law provides a maximum theoretical limit, at 59.3, to the mechanical efficiency of a wind turbine. Since wind turbines work by slowing down passing wind in order to extract energy, it would be impossible to gain a 100% efficiency since it would mean that all the wind would have to be stopped. Meaning that no wind would pass the wind turbine, causing the turbine to stop spinning. This will affect the design of the combined airfoil and actuator disc and give an idea of the expected theoretical limit.

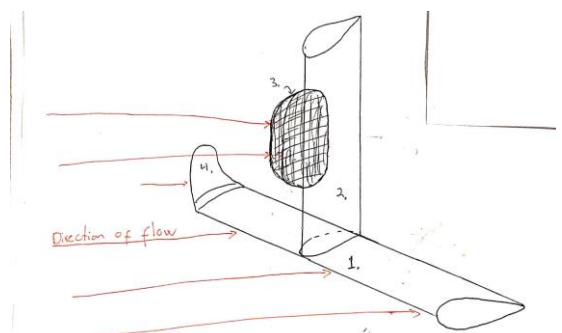


Figure 2-16, Concept hydrofoil that are to be tested

2.5 Scale-modelling

Physical models are intended to represent the full-scale system as close as possible. Modelling or scaling laws are needed to determine the properties and ensure a similar behavior of the model and the full scale.

Symbol	Dimensionless Number	Force Ratio	definition
Re	Reynolds Number	Inertia/Viscous	$\frac{UL}{\nu}$
F_N	Froude Number	Inertia/Gravity	$\frac{U}{\sqrt{gL}}$

Table 1, Scaling table

2.5.1 Froude Number

The dynamic similarity requirement applied on the ratio between inertia and gravity forces gives the following relation

$$\frac{F_i}{F_g} \propto \frac{\rho U^2 L^2}{\rho g L^3} = \frac{U^2}{gL}$$

Equation 4, Ratio between inertia and gravity forces

Applied on model and full scale this requirement gives:

$$\frac{U_M^2}{gL_M} = \frac{U_F^2}{gL_F}$$

$$\frac{U_M}{\sqrt{gL_M}} = \frac{U_F}{\sqrt{gL_F}} = F_N$$

Equation 5, Froude number

Geometrical and kinematic similarity, and equality in Froude number [Fn] in model and full scale will ensure similarity between inertia and gravity forces. Surface waves are gravity waves, this implies that equality in Froude number should give equality in wave resistance coefficient.

2.5.2 Reynolds Number

The equal ratio between inertia and viscous forces gives:

$$\frac{F_i}{F_v} \propto \frac{\rho U^2 L^2}{\mu UL} = \frac{\rho UL}{\mu} = \frac{UL}{\nu} = Re$$

Equation 6, Equality in Reynolds number

Equality in Reynolds number (Re) between full scale and model scale will ensure that the viscous forces are correctly scaled.

3. Experimental method

3.1 MarinLab

The experimental test has been conducted in MarinLab at Western Norway University of Applied Science in Bergen. The tow-tank at MarinLab has a length of 50m, width of 3.0m and a depth of 2.2m. The towing speed can be varied from $u=0 - 5$ m/s, over an effective towing length of 35 m.



Figure 3-1, Tow-tank at Western Norway University of Applied Sciences

3.2 Load Cells

A load cell is a device used to measure an applied force. They use one or more strain gauges, together with designed and machined components, to provide a linear change in resistance with the applied load. When an excitation voltage is input to the load cell, according to the bridge circuit, an output voltage is provided that is indicative to the applied load.



Figure 3-2, The load cells used in this experiment is made to measure forces as high as 10kg

3.2.1 Strain gauges

Strain gauges are wire or film resistors deposited on a thin, flexible carrier material. The wire or film is quite thin, so that it can easily be stressed. Strain is usually limited to about 10^{-3} . The first strain gauge was based on C. Wheatstone theory that the resistance of a wire changes due to mechanical stress and in 1938 E. E Simmons and A. C. Ruge developed, independently, the first strain gauge.

Strain gauges are suitable for the measurements of all kind of force-related quantities, for example normal and shear force, pressure, torsion, bending and stress. Strain gauges respond primarily on strain, $\frac{\Delta l}{l}$. By using Hooke's law, the applied force is found from the value of compliance or elasticity of the material on which the strain gauge is fixed. In practice there are two ways to apply strain gauges:

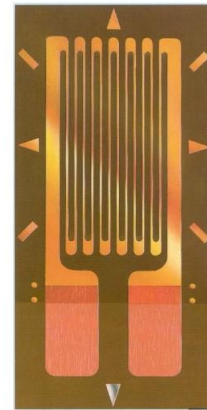


Figure 3-3 Basic design of a strain gauge

1. Directly mounted in the object whose strain and stress behavior must be measured; when cemented properly, the strain of the object is transferred ideally to the strain gauge.
2. Mounted on a specially designed spring element which the force is applied to. (load cell)

[30]

3.2.2 Dimensioning of the load cells

To find the right kind of load cells it is necessary to do some calculations to find what range of forces we will expect to find. This was done in an Excel file, where the complete file can be found in *attachment 1*. The equations were done by following the formulas for Lift, Drag, Reynold's number and areal. Certain assumptions were made, as the value of viscosity and density of the water. Constants C_L and C_D was retrieved from *airfoiltools.com* for different angle of attack, from negative 14 degrees to positive 14 degrees. [31]

$$Drag = \frac{(C_D * A * \rho * V^2)}{2}$$

Equation 7, Drag

$$Lift = \frac{(C_L * A * \rho * V^2)}{2}$$

Equation 8, Lift

$$Re = \frac{(cL * \rho * V)}{u}$$

Equation 9, Reynolds number

$$A = B * cL$$

Equation 10, Areal

Data:

Angle of attack = from -14 to 14 degrees

cL (chord length) = 0,135 m

B (wing width) = 0,8 m

V (velocity) = 4 m/s

ρ (density) = 1000 kg/m³

u (viscosity) = 0,0010518 Pa*s

By combining these formulas, max expected lift and drag can be calculated. These are important to know before choosing a load cell, to make sure that the load cell can measure the forces we expect to find. As shown in the attachment, the max expected lift is 134,88N, at 12.25 degrees, and max drag is 9,7N, at 14 degrees. It is also important to be aware that these equations were made solely on the presence of a NACA0012 hydrofoil, and that the numbers are not meant to be exact but to be used as a guidance.

3.2.3 Load Cell Calibration

Before use, the load cells and strain gauges need to be calibrated. This is done by following certain steps:

1. Repeatedly load and unload the balance, within the linearity range, to “age” the gauges.
2. Check insulation between gauges and balance body
3. Single component balance:
 - a. Zero check
 - b. progressively apply known load
 - c. Note output voltage, bridge supply voltage and amplifiers gain
 - d. Determine linear calibration curve:

$$\Delta E/E = \Delta R/R = k\Delta l/l = f(\text{load})$$

Equation 11, Calibration curve

4. Multi-component balance (N=2-6)
 - a. Same steps as above for each component independently, then for combinations of loads to determine interference.
 - b. Use calibration rig to proper multiple loads alignment
 - c. Determine calibration matrix NxN
 - d. Calibration matrix must be made non-dimensional with balance ranges, otherwise the comparison of matrix terms for forces and moments is meaningless.

[32]

3.3 Wingtips

Winglets improve efficiency by diffusing the shed wingtip vortex which in turn reduces the drag due to lift and improves the wing's lift over drag ratio. [33] As mentioned in *chapter 2.3* the advantage off adding winglets need to bigger than the weight it adds. To optimize the effect of winglets it is important to take in consideration the individual object and the angle of the winglet. Many researches have been done to find the best geometry for winglets. A Japanese study published in the *Journal of aircraft* concluded that the large cant angle (*the angle between the wingtip and the vertical axis*) of the winglet was found to be favorable. [34] Oklahoma State University did a study on winglet on UAVs. In this study the blended winglet with the highest cant angle tested gave the best lift-to-drag ratio. [35]

In this study the wing will be tested with three different wingtips: A, B and C

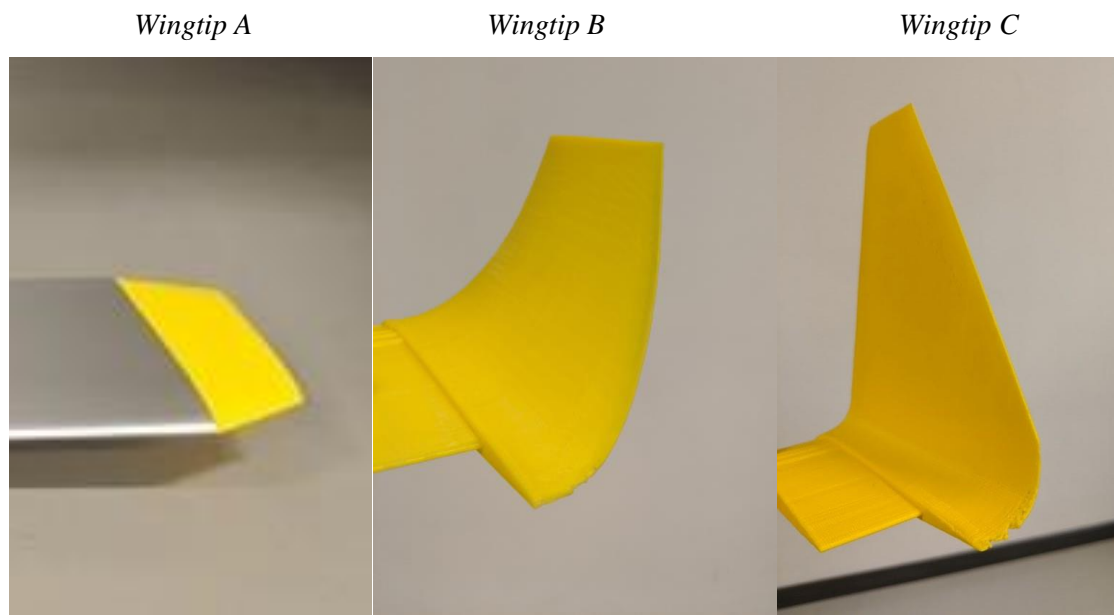


Figure 3-4, Wingtip A, B and C is all used in the experiment

Wingtip A is just an extension of the wing. Wingtip C is a winglet that's have a cant angle at zero degrees, which in this thesis is set to the angle from the vertical axis. Wingtip B is also a winglet, and it is a mixture of wingtip A and C with a cant angle bigger than C.

3.4 Force measurements

A load cell is used to measure the forces working on the hydrofoil. The load cell configuration is made to measure forces working horizontally, drag, and vertically, lift, on the hydrofoil wing. The load cells where implemented into the construction shown in

Figure 3-5. The load cell construction is made up of two sections, one section for each load cell, where each section will only be able to move in one given direction. Making it great for measuring the forces working in that given direction.



Figure 3-5, The load cell configuration can measure forces in horizontal and vertical direction

The load cell configuration will be used to measure lift and drag forces on the hydrofoil at different angles of attack, different winglets and different velocities.

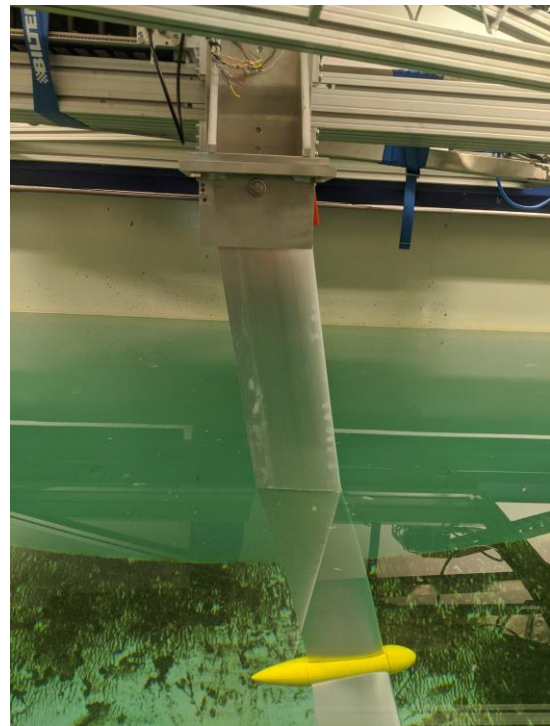
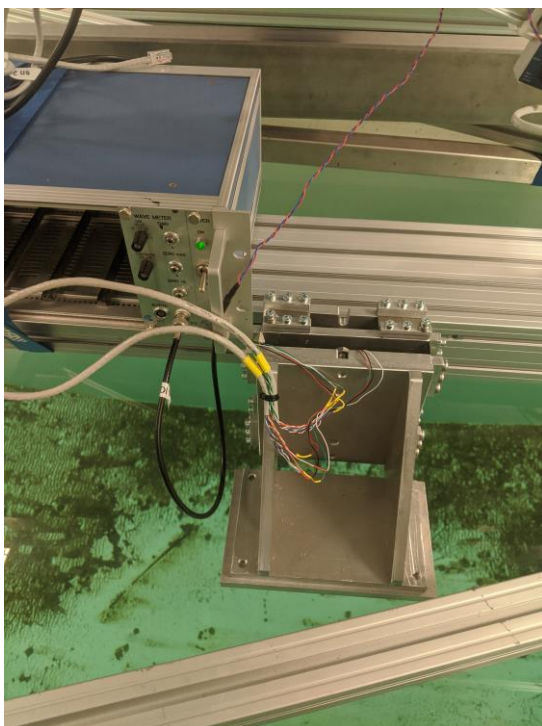


Figure 3-6, The load cell is mounted on the drag-wagon with the hydrofoil connected underneath

The load cell configuration will then be mounted on a tow-wagon, which moves along the pool, with the hydrofoil mounted underneath. When the tow-wagon moves, the forces working on the hydrofoil will be registered on the load cells.

3.5 Test matrix explanation

The main reason behind the test matrix is to log all data that are received during the lab test. The importance behind a good test matrix cannot be stressed enough and could be the difference between a good lab test and a poor one. The test matrix will log all different measurements, and all the different test runs. Making it efficient and straightforwardly.

TestSet#	Winglet	Drag Disc	AOA	0.5 m/s			1 m/s			1.5 m/s			2 m/s		
				Number of tests	Lift #1	Drag #2	Number of tests	Lift #1	Drag #2	Number of tests	Lift #1	Drag #2	Number of tests	Lift #1	Drag #2
1,1	A	none	0												
1,2	A	none	5												
1,3	A	none	10												
1,4	A	none	15												
1,5	A	1	0												
1,6	A	1	10												
2,1	B	none	0												
2,2	B	none	5												
2,3	B	none	10												
2,4	B	none	15												
3,1	C	none	0												
3,2	C	none	5												
3,3	C	none	10												
3,4	C	none	15												

Figure 3-7, Test matrix

As shown in Figure 3-7, which shows the test matrix, the different kinds of tests are labeled. They show what is to be tested, what speed it is tested at, what type of winglet, with or without drag disc and lift and drag. Each test is also marked with an individual test set number, making it easy to track and adjust after the tests are completed. Each test will be saved as a text file, with a unique code to distinguish the different tests from each other. An example of how the test will be labeled is: *u0_a10_A_01*, where *u* describes the velocity tested, *a* describes angle of attack, *A* describes type of wingtip and *01* describes test number.

3.6 Potential error sources

There are different potential error sources that can cause problems during the testing. Some of them are human errors and others are equipment errors. It is important to be aware of the different potential errors so that they can be avoided, and so that the results from the tests are as correct as possible. Some of the potential error sources are:

1. Incorrect measurements
2. Equipment failure
3. Human error

3.7 Lab procedure

3.7.1 Assemble hydrofoil

First step is to assemble the hydrofoil. The prototype is made up of three hydrofoils, two horizontal and one vertical. The prototype will be tested with different winglets, mentioned in chapter 3.3, and with a drag disc.

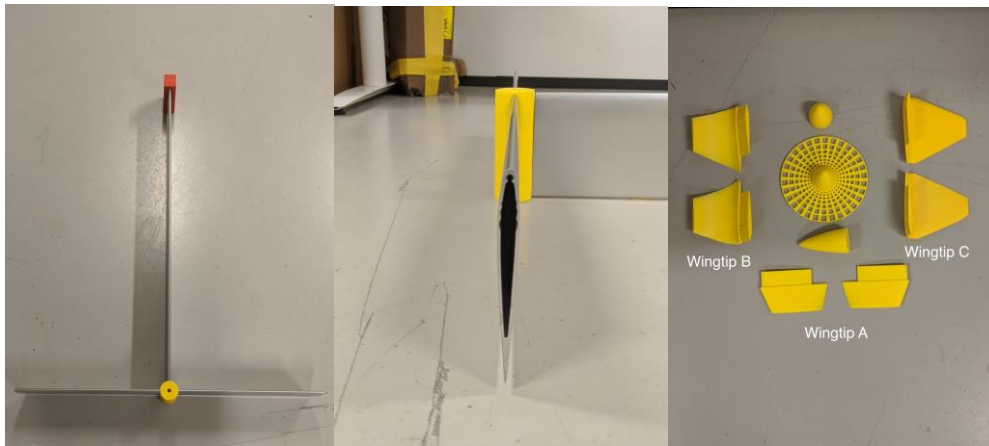


Figure 3-8, Hydrofoil parts, showing the wing, different types of winglets and the drag disc

3.7.2 Calibrate load cells

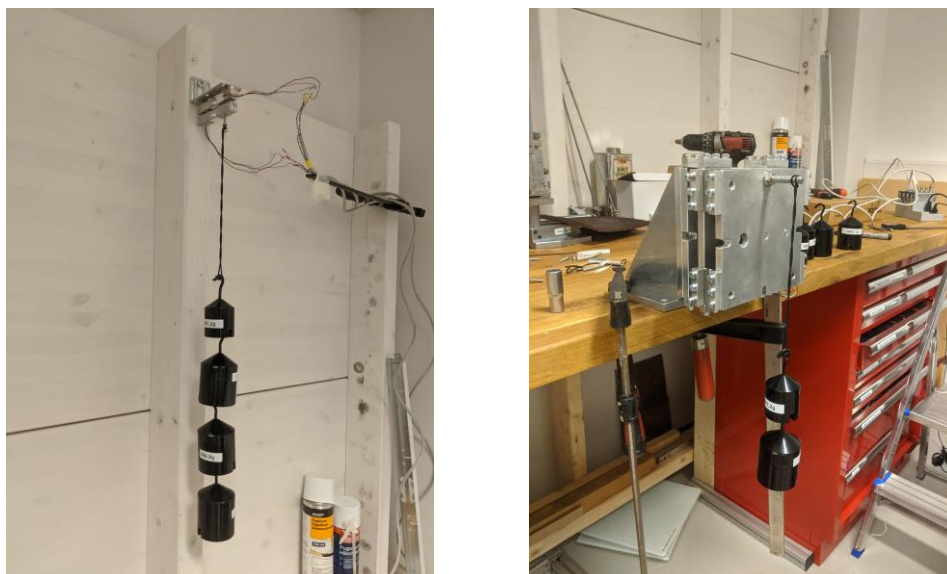


Figure 3-9, Calibrating the load cells before and after assembly, using weights

The two load cells (one for lift, one for drag) have to be calibrated separately. This is done by loading them with 10 different weights and measuring the voltage signal of the load cell. A calibration factor k [Newton/Volts] can be calculated from a linear interpolation of the voltage signal to the strain.

3.7.3 Connecting to tow-wagon

Then the load cell is mounted onto the towing-wagon, before connecting the prototype to the load cell. When connected to the towing-wagon the depth of the hydrofoil, underneath the water surface, is ranging between 54cm (for $\alpha = 15$) and 58cm (for $\alpha = 0$), depending on angle of attack.

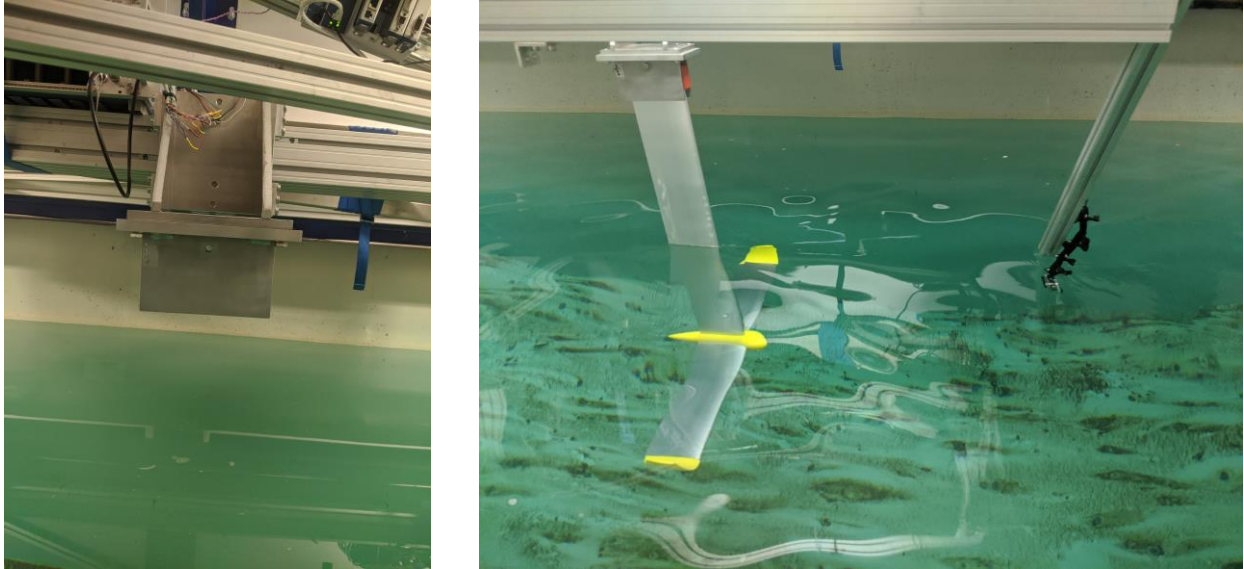


Figure 3-10, The load cell is mounted onto the tow-wagon, and the prototype onto the load cell

3.7.4 Testing

Then several tests are done with different velocities, different angle of attacks and different winglets. Some of the test are done several times, to quantify the data received.

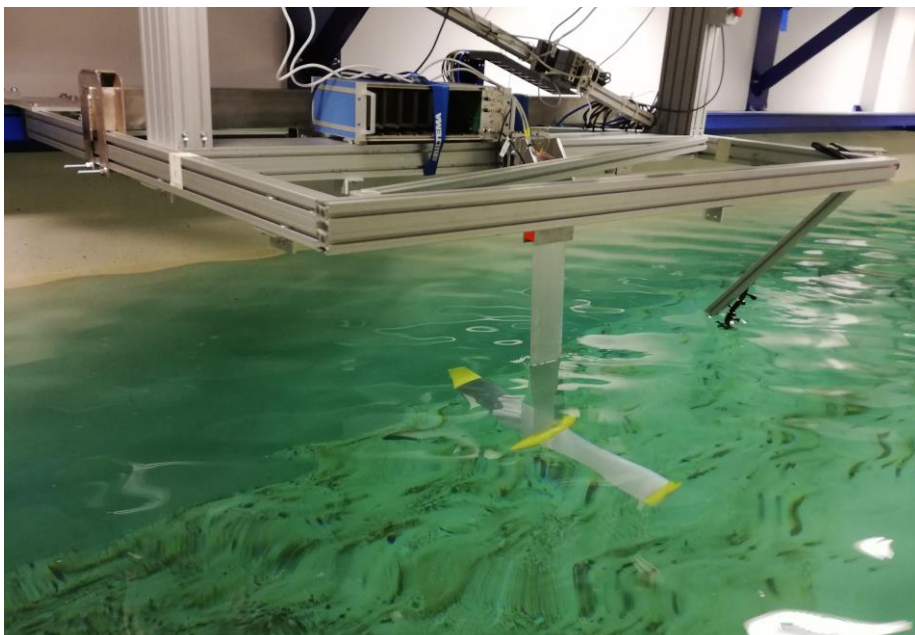


Figure 3-11, The tow-wagon moves across the pool and inflicting forces upon the hydrofoil

3.7.5 Deviation in angle of attack

After mounting the prototype and the load cell unto the tow-wagon a deviation in the angle was found. Therefore, measurements of each angle were made to quantify the real angle tested.

At angle “0” =

$$\tan^{-1}\left(\frac{0,8}{58,5}\right) = 0,78355^\circ$$

At angle “5” =

$$\tan^{-1}\left(\frac{5,7}{58,5}\right) = 5,565^\circ$$

At angle “10” =

$$\tan^{-1}\left(\frac{10,7}{58,5}\right) = 10,365^\circ$$

At angle “15” =

$$\tan^{-1}\left(\frac{16,1}{58,5}\right) = 15,387^\circ$$

3.8 Reynolds number in the tow-tank

The Reynolds number is a product of the temperature of the water and the velocity of the tow-wagon. The water temperature was measured to be at 16.8°C, giving us a kinematic viscosity of 0.000001086 m²/s. [36]

$$\text{Reynolds number} = \frac{vl}{\nu}$$

Equation 12, Reynolds number

Data:

v = Velocity of the fluid

l = The chord length of an airfoil

ν = Kinematic viscosity of the fluid

[37]

4. Theoretical method

A excel document, *appendix 2 - Analytical model of hydrofoil assembly*, was made to calculate lift- and drag forces for different angle of attacks at different velocities. An excel sheet was also made to calculate the geometric design needed to be able to lift the wind turbine into flight-mode at startup speed. Each calculation shows what forces is expected to work on the full-scale wind turbine, at different velocities.

4.1 Geometric design and data

These sheets are used to calculate lift-force at a given start-up speed, wind velocity at 3,5 m/s. The *Geometric Data* sheet is used to calculate the tip-speed-ratio of the hydrofoil. This result is then used in the *Geometric Design* sheet. In the *Geometric Design* sheet calculations of lift is done to determine the necessary design of the hydrofoil. The start-up speed, *TSR_Hydrofoil* and the necessary lift-force needed is crucial to be able to determine the design. On top of the sheet *Geometric Design* some assumptions and demands are mentioned. The sheet is then divided into three parts, the calculations for an *AOA of 5*, *AOA of 10* and *AOA of 15*.

The full-scale wind turbine has a vertical hydrofoil which is made up by four separate hydrofoil types, from the end to start, a NACA0012, NACA0015, NACA0018, NACA0021. Chord lengths and lengths of each section can be found in *attachment 2*, as well as the lift coefficient.

4.1.1 Assumptions and demands

Assumptions:

- Reynolds number over one million has little to none effect on the lift coefficient.
- The turbines TSR = 3,4

Demands:

- Angle of attack varies from 5 to 15 degrees
- Velocity of the wind equals 3,5 m/s (start-up-speed)
- The length of each part of the hydrofoil is based on a percentage of the total length. (Section 1 is 9,1% of total length)
- The wing is made up of 6 sections (each hydrofoil consists of two horizontal wings)
- Necessary lift force needed is 826700 Newton

4.1.2 Steps

To do the calculations on the *Geometric Design and Data* sheets, following steps were made

- I. Find the necessary force needed for the wind turbine to go into flight-mode
 - a. Is given to be 826700 Newton by MantaWind AB
- II. Find the tip-speed-ratio for the hydrofoil
- III. Find the velocity of the hydrofoil by using the tip-speed-ratio
- IV. Find the forces working on each section of the horizontal hydrofoil
- V. Check if the total lift-force is higher than the necessary force needed for the wind turbine to go into flight-mode

4.1.3 Calculations

Tip-speed-ratio of the hydrofoil

Data:

$$TSR_{at R=65m} = 3,4$$

$$R_{Turbine} = 65m$$

$$R_{Hydrofoil} = 49,13m$$

$$TSR_{Hydrofoil} = \frac{R_{Hydrofoil}}{R_{Turbine}} * TSR_{at R=65m} = 2,57$$

Equation 13, Tip-speed-ratio

Startup-speed

Data:

$$TSR_{Hydrofoil} = 2,57$$

$$Wind\ Velocity_{Start-up} = 3,5\ m/s$$

$$Hydrofoil\ Velocity_{Start-up} = TSR_{Hydrofoil} * Wind\ Velocity_{Start-up} = 8,995\ \frac{m}{s}$$

Equation 14, Start-up velocity for the hydrofoil

Lift-forces working on each section of the hydrofoil at start-up velocity, AOA from 5-15

Uses the formula for *Lift*, given in equation 6, to calculate lift-forces working on each section of the hydrofoil.

Data:

$$\text{Hydrofoil Velocity}_{\text{start-up}} = 8,995 \text{ m/s}$$

$$\rho = 1025 \text{ kg/m}^3$$

C_l = Given by Airfoiltools.com for each section

A = Length in spanwise direction * Chord length

4.2 Calculations of angle of attack

The four excel sheet, AOA0, AOA5, AOA10 and AOA15 calculates lift and drag forces working on each section of the wind at different velocities. Wind velocity varies from 2m/s, and ends on a wind velocity at 11,9 m/s. These calculations show the total lift from the horizontal hydrofoil, total drag, total drag for both the vertical and horizontal wing, as well as lift-to-drag ratios.

The calculations are for the full-scale Manta Wind Turbine and hydrofoil assembly.

To find lift and drag forces working on each section, Equation 7, *Drag*, and Equation 8, *Lift*, is used.

Lift-to-drag ratio

$$\frac{\text{Total Lift}}{\text{Total Drag}} = \text{Lift - to - drag ratio}$$

Equation 15, Lift-to-drag ratio

5. Result

5.1 Theoretical result on the full-scale wing section

Theoretical results show calculations based upon a full-scale Manta Wind turbine. Calculations can be found in *attachment 2*. Each figure shows total forces, in newton, working on each hydrofoil on the full-scale wind turbine.

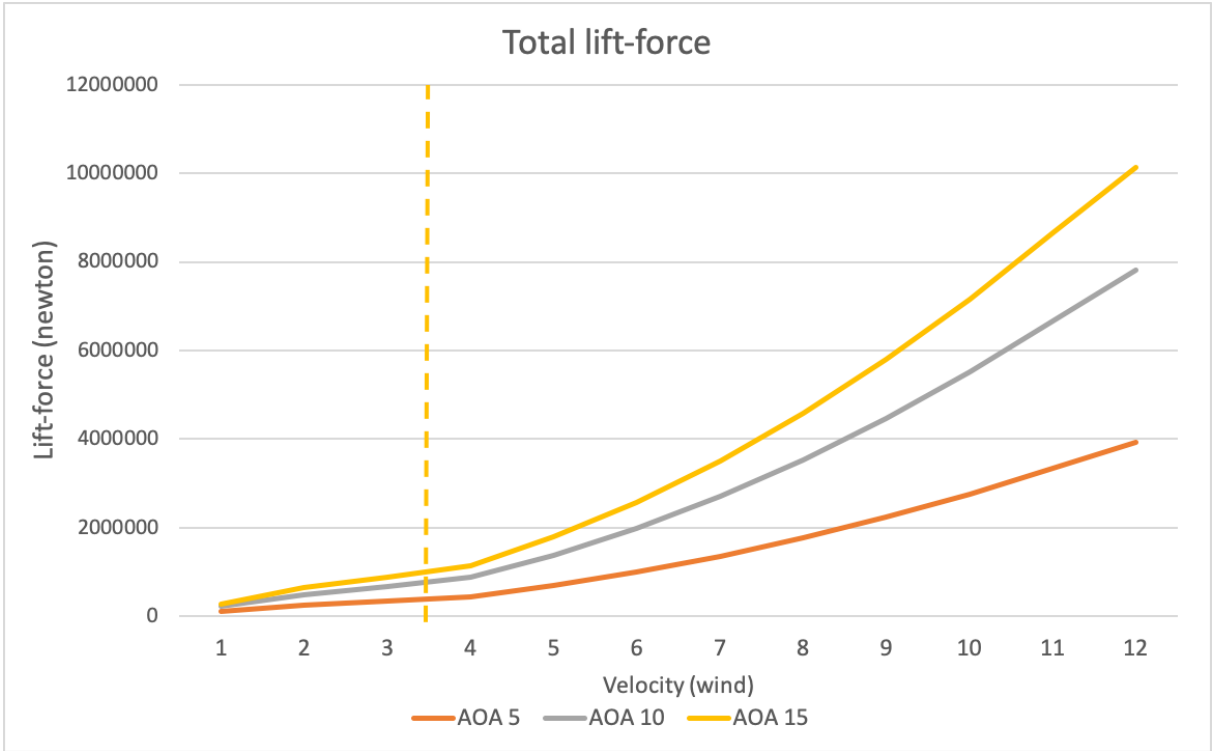


Figure 5-1, Total lift-force on the full-scale Manta Wind turbine for different velocities, the yellow stippled-line showing start-up-speed.

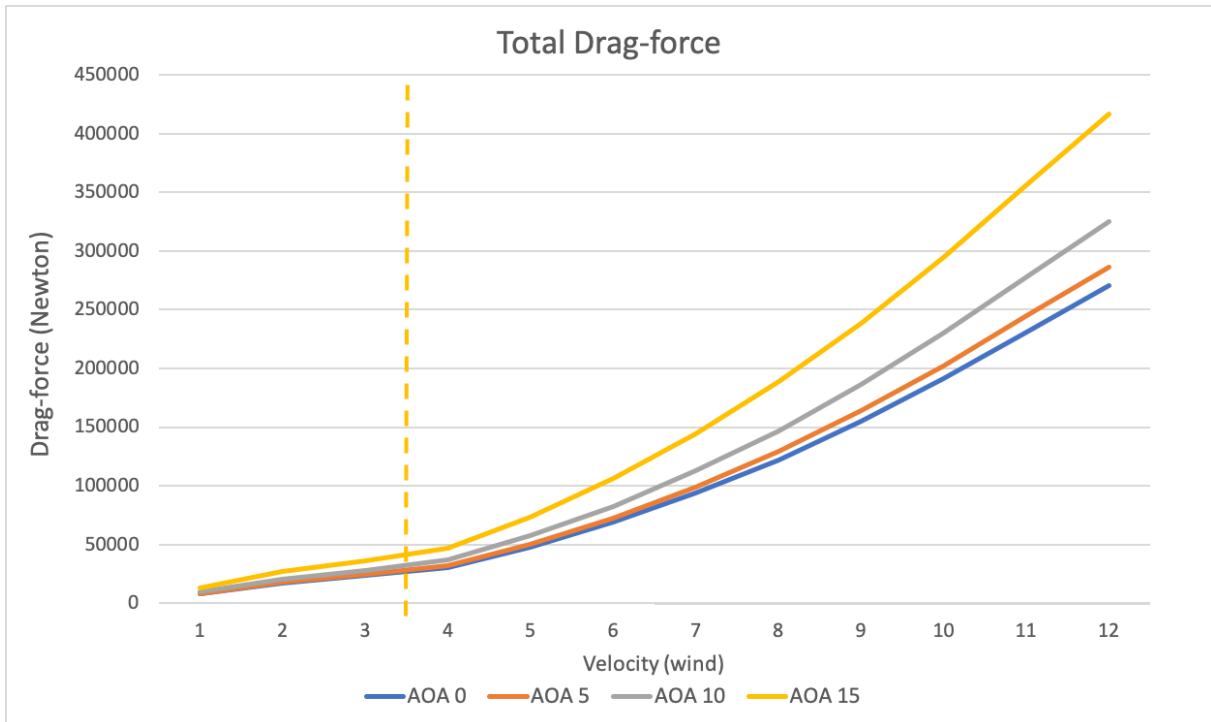


Figure 5-2, Total Drag-force on the full-scale Manta Wind turbine for different velocities, the yellow stippled-line showing start-up-speed.

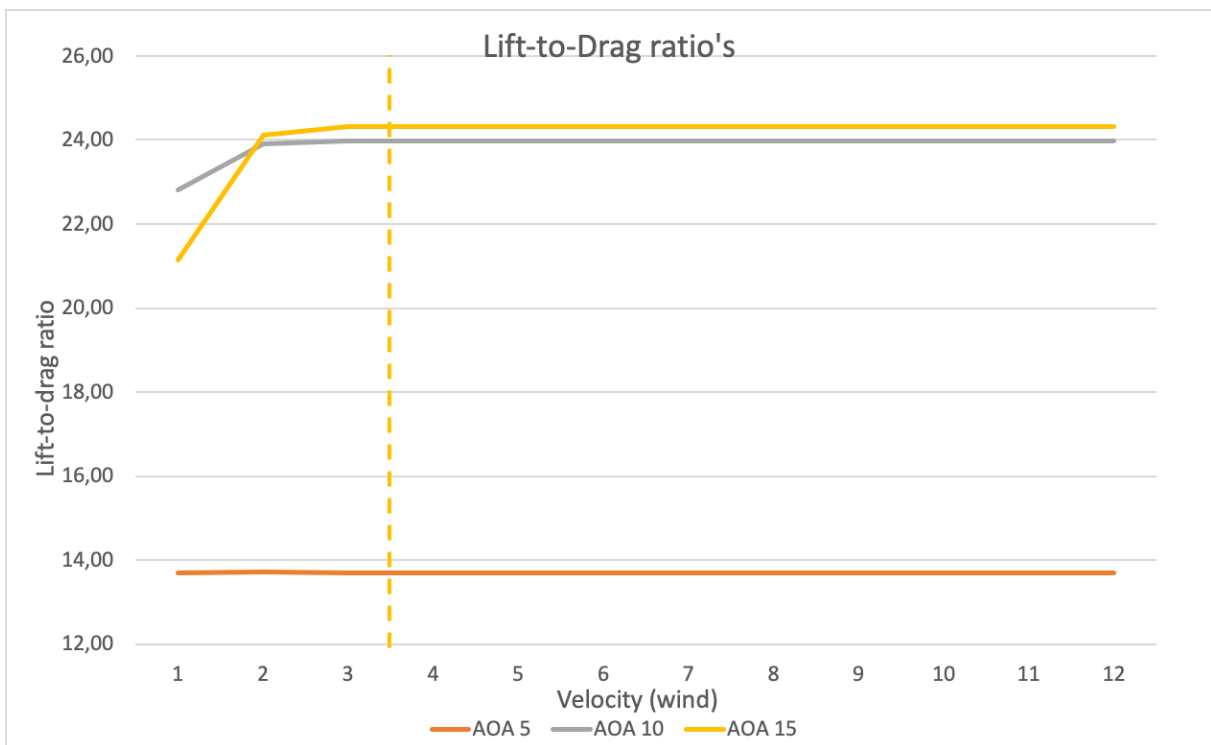


Figure 5-3, Lift-to-drag ratios on the full-scale Manta Wind turbine for different velocities, the yellow stippled-line showing start-up-speed.

As mentioned in chapter 4.1, the full-scale Manta Wind turbine consists of different kinds of hydrofoils, which is combined into one. The figures above shows that at angle of attack at 10 degrees or 15 degrees, gives the best lift to drag ratios. These calculations do not consider factors as stall, underwater currents and other natural phenomena, and is purely based on theoretical data.

	Section 1	Section 2	Section 3	Section 4	Section 5	Section 6
Length in spanwise direction (m)	0,5	1	1	1	1	1
Chord length (m)	0,6	1,1	1,4	1,5	1,6	1,7
Profile	Naca0012	Naca0012	Naca0012	Naca0015	Naca0018	Naca0021
Cl	1,1046	1,1046	1,1046	1,1091	1,0998	1,0093
Cd	0,01364	0,01364	0,01364	0,01473	0,01412	0,01368
Lift-force (N)	12943,61	51774,42	62129,31	67580,95	72169,21	70961,33
Drag-force (N)	159,83	639,33	767,20	897,55	926,56	961,81

Table 2, An excerpt from appendix 2, showing theoretical calculations for wind velocity at 3,5 m/s and angle of attack at 10 degrees. Showing the different sections of the wing, where section 1 is the wingtip and section 6 is in the center by the hub.

5.1.1 Manta Wind dimensions, based upon start-up velocity

<i>Angle of Attack</i>	<i>Hydrofoil length (half of the wing)</i>	<i>Median chord length</i>
5	5,5 m	>3,4 m
10	5,5 m	>1,6 m
15	5,5 m	>1,3 m

Table 3, Showing median chord length needed to lift the turbine into "flight-mode" at different angle of attacks and wind velocity at 3,5m/s

Both hydrofoil length and the median chord length may be changed in *attachment 2*, to get the right dimensions.

5.2 Experimental results on the model-scale wing section

In the following chapters the results from the experimental tow-tests on the model-scale wing section are presented.

5.2.1 Lift and Drag force timeseries

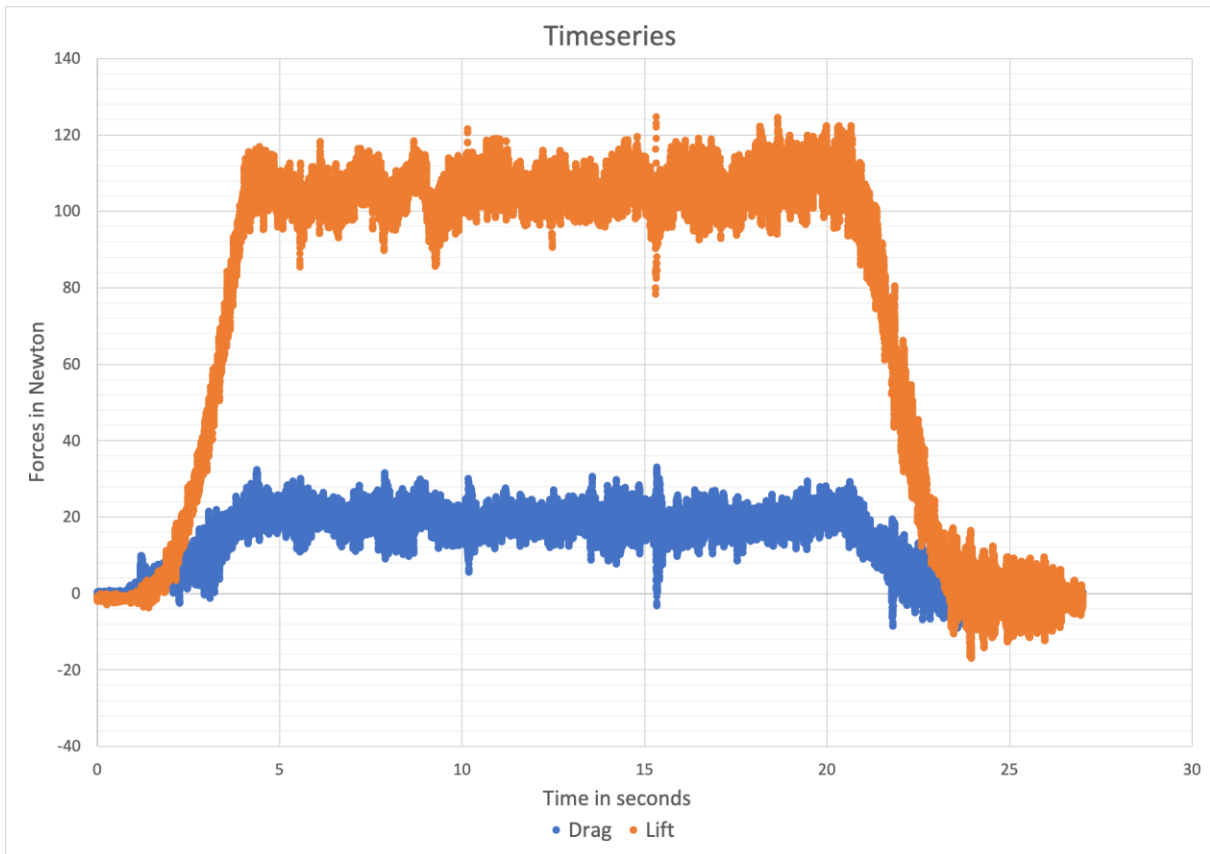


Figure 5-4, Timeseries showing the raw data recovered from a test at velocity = 1,5m/s, angle of attack = 10 degrees and with winglet A

Figure 5-4 shows a typical test run done in the tow-tank in Western Norway University of Applied Science MarinLab. The different test is done over a length of 30meters, and varies in velocity tested, angles tested, and winglets added. Each test run varies in length of time due to the velocity. The load cell records two thousand points of measurements per second, which equals to a thousand measurement points on lift-forces, and thousand on drag-forces.

The constant lift and drag data that can be found after the acceleration and before the de-acceleration is the one used for calculating the time-averaged lift and drag forces. This data gives an understanding of what forces will be functioning on the hydrofoil at a given Reynolds number. In Figure 5-4 this equals to the data between 5 seconds and 20 seconds. This time interval gives a deviation in forces measured; therefore, an average force value is calculated. If several tests are done at the same test conditions, an average value of the average forces is calculated. Giving the most accurate values.

5.2.2 Comparison Experiment vs theory

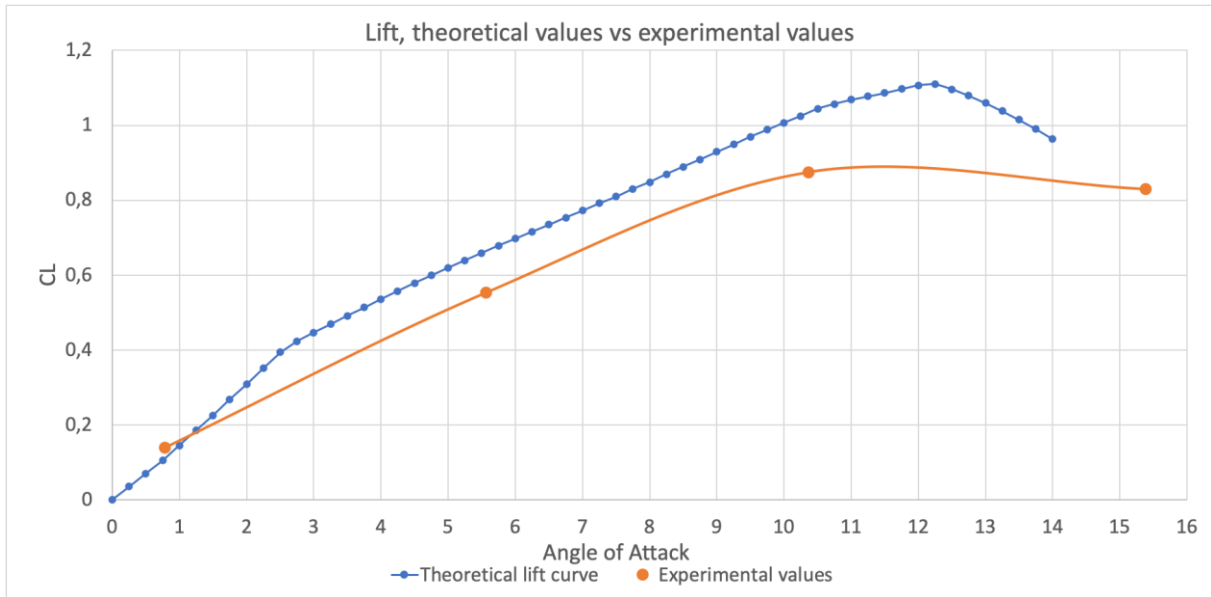


Figure 5-5, Comparing theoretical lift-values with experimental lift-values at velocity = 1,5m/s and winglet A

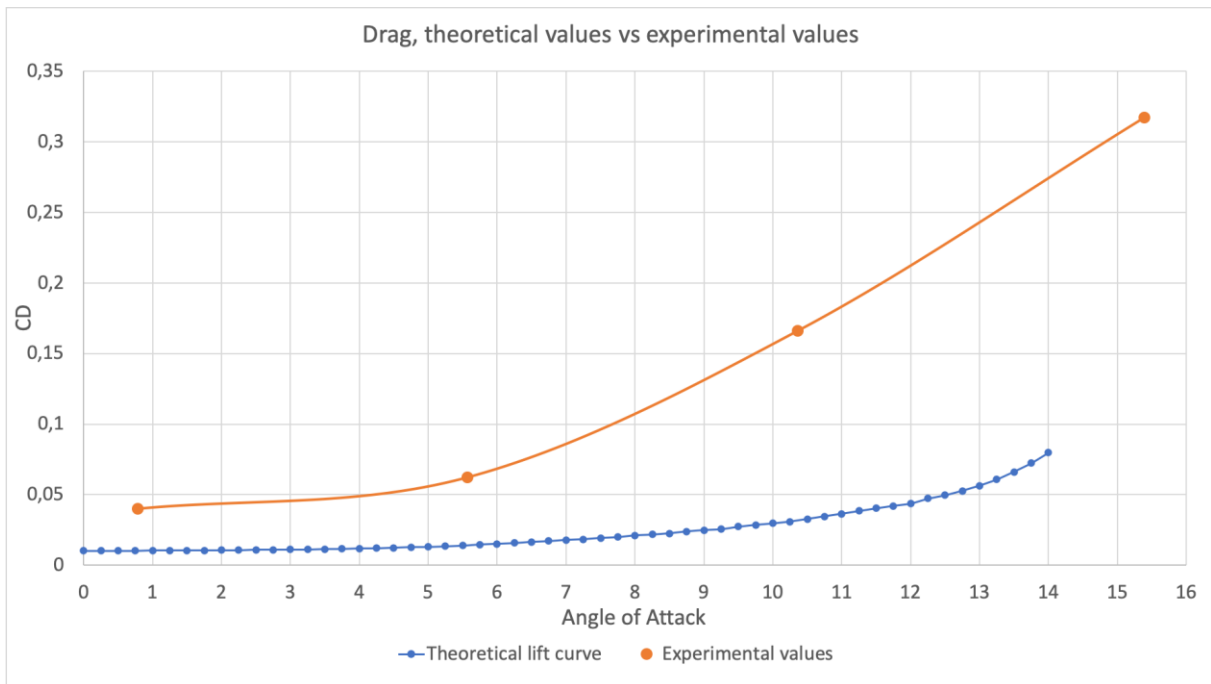


Figure 5-6, Comparing theoretical drag-values with experimental drag-values at velocity = 1,5m/s and winglet A

The theoretical values are taken from airfoiltools.com at Reynolds number at 1million, and a turbulent flow. This data equals the Reynolds number at the experimental test run at velocity = 1,5m/s.

As shown in the figures above the theoretical values differs from the experimental values. It is observed that the measured lift values are smaller than the theoretical values, while the experimental drag values are larger than the calculated ones. This is due to different factors as:

1. Effects of stall are difficult to predict by simplified theoretical calculations, which explains the deviations in both lift and drag at $\alpha=15$.
2. The theoretical calculations are based only on a horizontal wing section of a Naca0012 foil. The vertical part is not considered in the theoretical calculations but is assumed to contribute with a significant amount of drag in the experiment.
3. The density of the fluid which the prototype was tested in, might differ from the density used in the theoretical calculations. This is however considered to only have a small contribution.
4. Reduced lift and increased drag due to flow separation at the wing tips was not considered in the theoretical calculations

5.2.3 Comparison of wingtip configurations

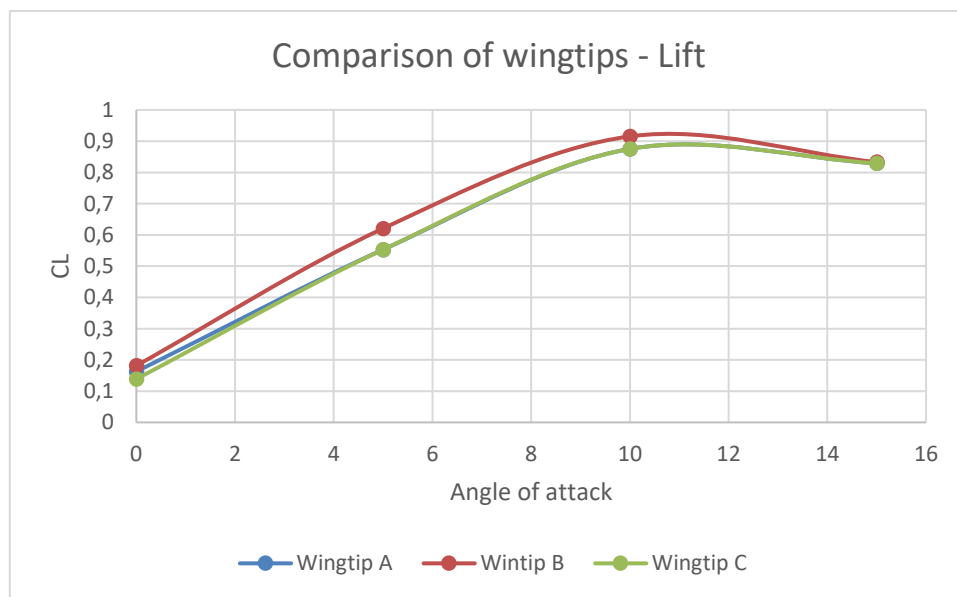


Figure 5-7, Different types of wingtips compared for lift at different angles. Velocity at 1,5m/s

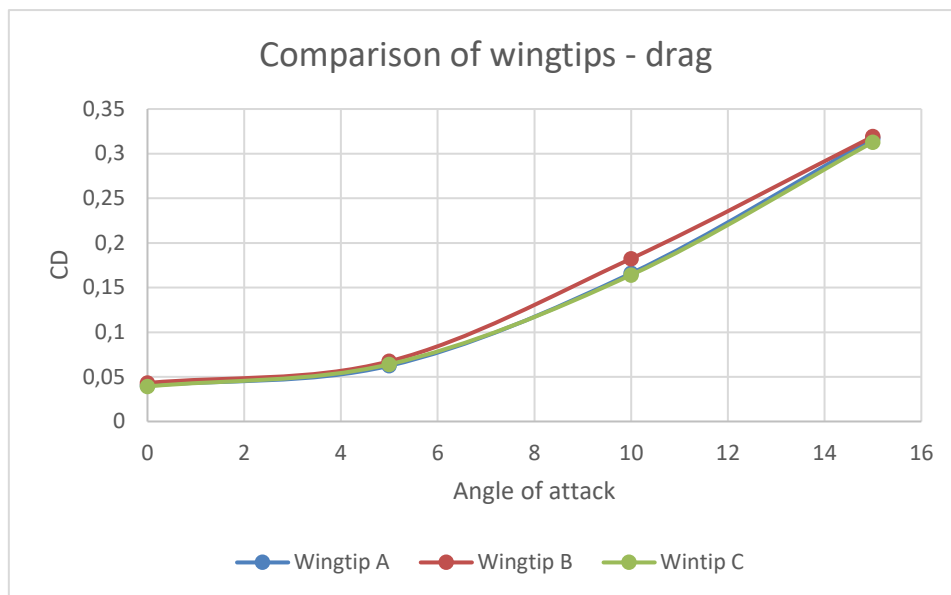


Figure 5-8, Different types of wingtips compared for drag at different angles. Velocity at 1,5m/s

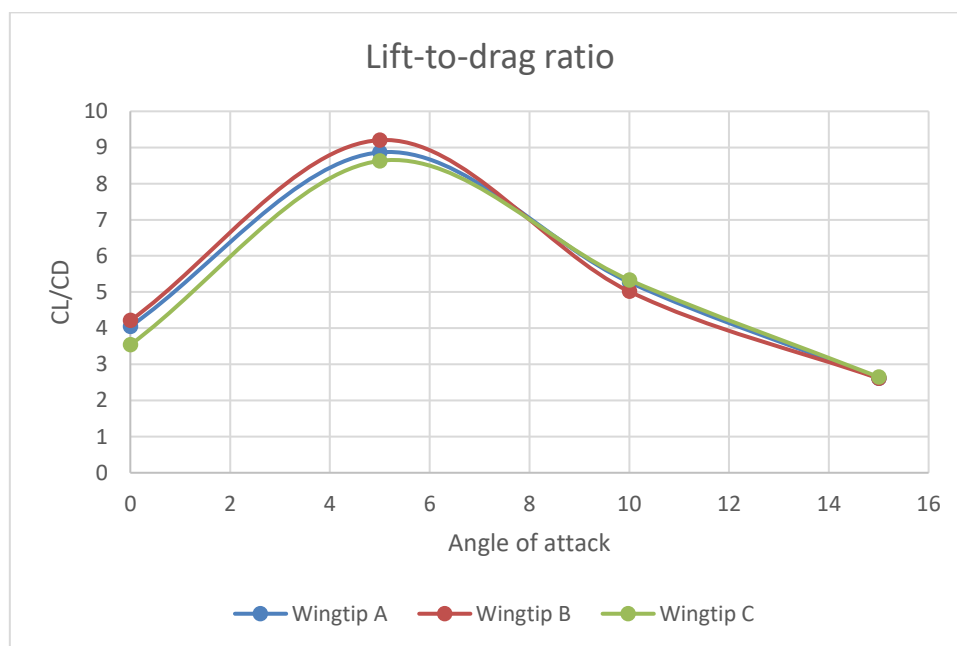


Figure 5-9, Lift-to-drag ratio for different wingtips at velocity at 1,5m/s

In Figure 5-7 and Figure 5-8 a comparison of different wingtips is shown. The different types of winglets are mentioned in chapter 3.3. In this experiment wingtip B gives the highest lift coefficient. This indicates that a winglet is effective for increasing lift. However, larger winglets are not necessarily increasing lift as wingtip C shows a smaller lift than Wingtip B even though its bigger. Drag coefficient is almost similar between wingtip A, B and C. Wingtip A gives the smallest, which can be explained due to its smaller surface area. The wing tested in the tow-tank is downscaled, and the difference between the wingtips will show more clearly in a full-scale model. By comparing the lift- and drag coefficient winglet gives a slightly higher lift-to-drag ratio.

5.2.4 Effect of Reynolds number

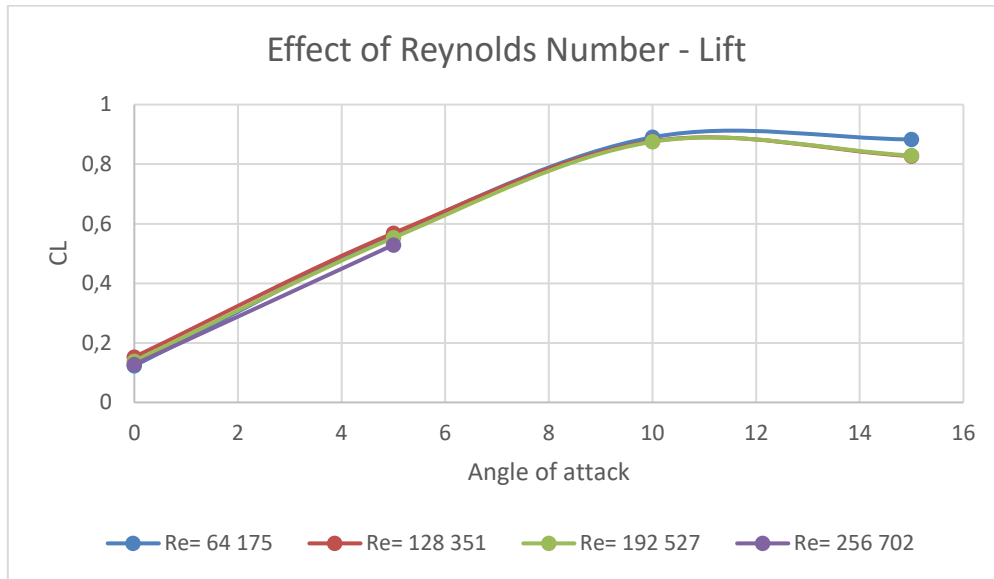


Figure 5-10, Comparing what the effect of Reynolds number has to say for the lift coefficient. Winglet type A

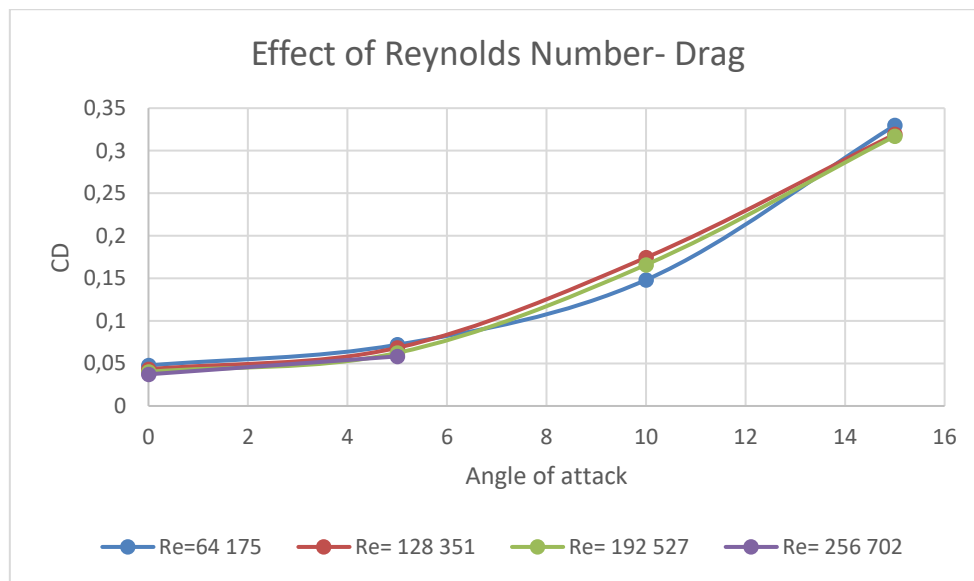


Figure 5-11, Comparing what the effect of Reynolds number has to say for the drag coefficient. Winglet type A

Comparing the lift- and drag coefficient by Reynolds number, the coefficient should be the same for every test despite the difference in Reynolds Number. The results show matching lift curves for all four Reynolds numbers tested. This could be explained by the equations for both of the two factors. The difference between the tests with different Re-number comes from uncertainty and noise in the measurement as well as other error sources.

5.2.5 Effect of disc-wing interaction

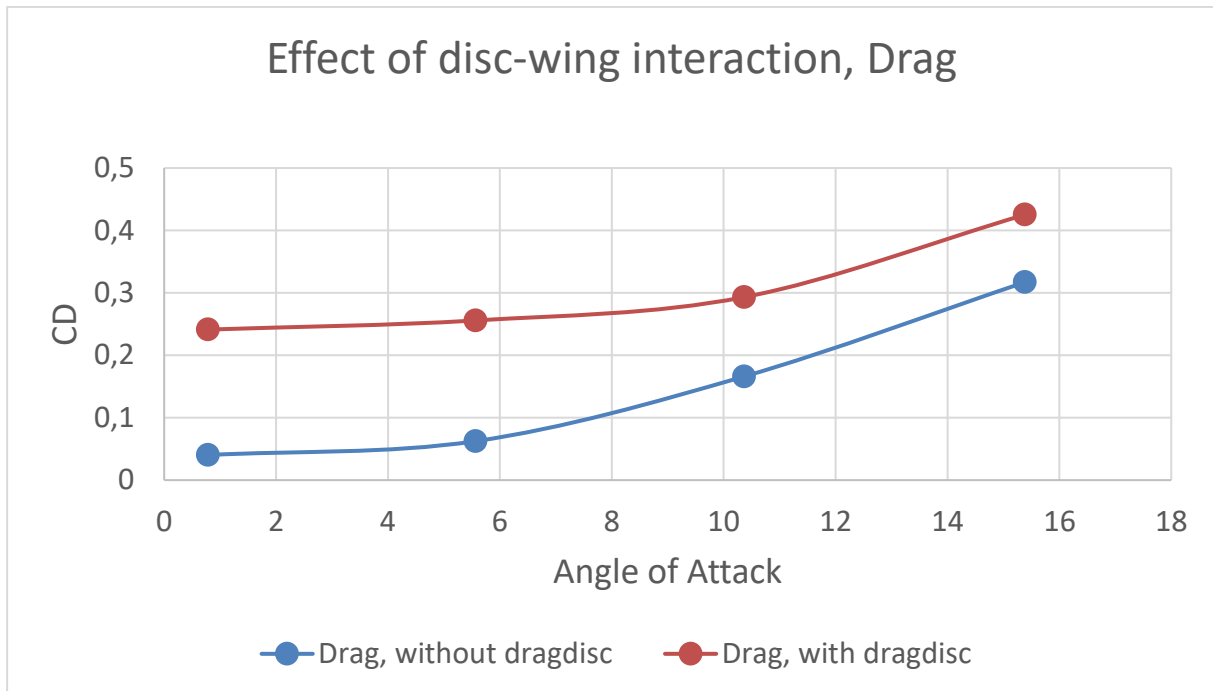


Figure 5-12, Comparing the effect of a disc-wing interaction for drag-forces at velocity = 1,5m/s and winglet A

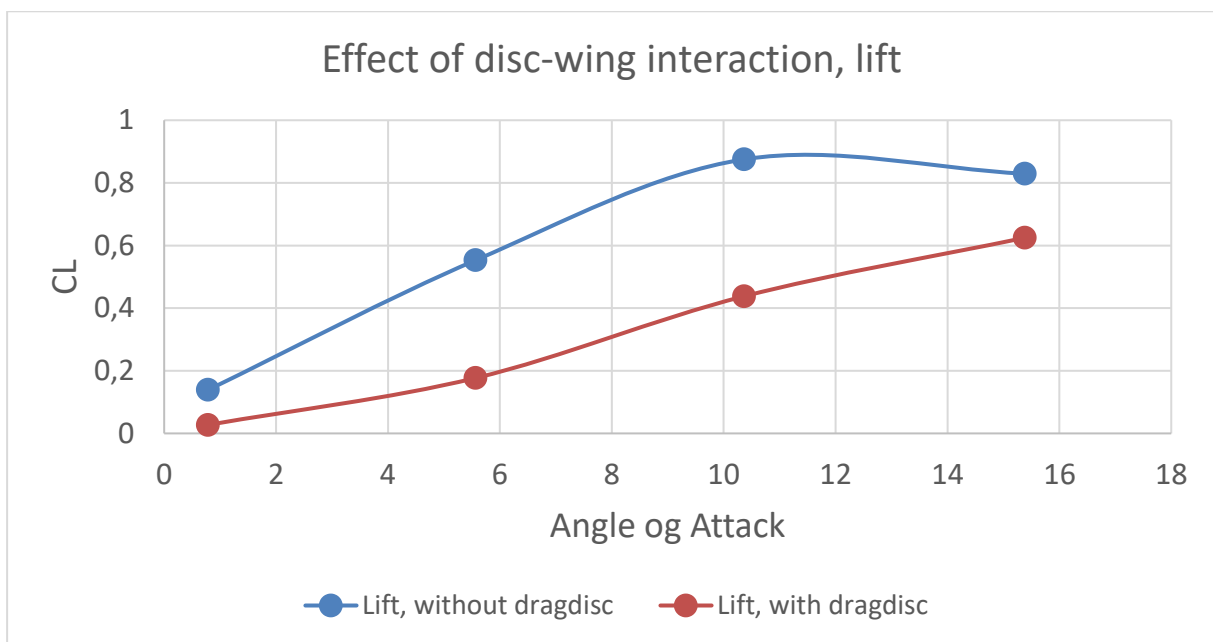


Figure 5-13, Comparing the effect of a disc-wing interaction for lift-forces at velocity = 1,5m/s and winglet A

The full-scale Manta Wind turbine will have water turbines attached to the hydrofoils. This will affect both drag and lift, as shown in Figure 5-12 and Figure 5-13. This corresponds with earlier theory, given in chapter 2.4.2, which mentions that the total lift force will decrease compared to when there is no turbine/disc at all. The increased drag is wanted and used to transform the kinetic energy to electricity.

6. Conclusion

Theoretical calculations and experimental tests have been done on a hydrofoil-wing which is a part of a Vertical axis wind turbine. Three different wingtip configurations and a drag disc have been tested on the wing. To get the test results as accurate as possible an average of the measuring points in a specific interval have been chosen. Comparing three different wingtips shows that the difference in drag-coefficient is very small. Wingtip B gave the highest lift-coefficient and highest lift-to drag ratio. By comparing different velocities, giving us a different Reynolds number, at a single wingtip configuration, one can see that the differences in Reynolds number has almost no effect on lift and drag coefficient. The drag disc on the other hand effect the coefficients a lot. The test gives a much lower lift-coefficient and a much higher drag-coefficient.

Comparing the theoretical and experimental results, on the prototype, one can see that the theoretical gives little higher lift-coefficient which can be explained by different density, stall, flow separation at the wingtips and that the theoretical calculations only looks at a single horizontal hydrofoil, not the complete prototype. The drag-coefficient is much higher in the experimental test, this is mostly because there is a vertical hydrofoil which effect the drag.

In this thesis, wingtip B, which is the winglet with largest cant angle, was the one who gave the best results in the tow-tank. The presence of the drag-disc resulted in a drag increase of more than 200% for alpha 0,5 and 10, while the lift was measured to be decreased by more than 50% for the same range of alpha.

To conclude, the finds in this thesis shows that a hydrofoil equipped with wingtip B will produce a higher lift-to-drag ratio and combined with a turbine/drag-disk an increase in drag will occur. This increased drag is wanted and will be used to transform the kinetic energy, in water, to electric energy. Combined, wingtip B and the drag-disk will give the highest desired lift-to-drag ratio.

7. References

- [1] Wind Europe, "Floating Offshore Wind Energy - A policy blueprint for Europe," [Online]. Available: <https://windeurope.org/wp-content/uploads/files/policy/position-papers/Floating-offshore-wind-energy-a-policy-blueprint-for-Europe.pdf>. [Accessed 21 May 2020].
- [2] Manta Wind AB, "MantaWind," [Online]. Available: <http://www.mantawind.com/>. [Accessed Februar 2020].
- [3] Alibaba Cloud Computing, "Evisdom," 2017. [Online]. Available: <http://www.evisdom.com/industri/2014/05/Hva-er-de-forskjellige-typene-av-vindmolle-Design.html>. [Accessed February 2020].
- [4] Rinkesh, "Conserve Energy Future," [Online]. Available: <https://www.conserve-energy-future.com/verticalaxiswindturbines.php>. [Accessed February 2020].
- [5] Klein-Windkraftanlagen, "Vertikale Windkraftanlagen," [Online]. Available: <https://www.klein-windkraftanlagen.com/technik/vertikale-windkraftanlagen/>. [Accessed February 2020].
- [6] N. E. Bassam, P. Maegaard and M. L. Schlichting, "Distributed Renewable Energies for Off-Grid Communities," Elsevier, 2012, pp. 111-123.
- [7] M. Ragheb, "Vertical Axis Wind Turbines," 2015.
- [8] P. Breeze, "The Anatomy of a Wind Turbine," in *Wind Power Generation*, Academic Press, 2016, pp. 19-27.
- [9] H. J. Sutherland, D. E. Berg and T. D. Ashwill, "A Retrospective of VAWT technology," Sandia National Laboratories, Albuquerque and Livermore, 2012.
- [10] R. Wilson, "Vortex Sheet analysis of a Giromill," *ASME Journal of Fluids Engineering*, 1978, pp. 340-342.
- [11] M. P. Boyce, "Gas Turbine Engineering Handbook (4th Edition)," Elsevier, 2012.
- [12] M. O. Hansen, *Aerodynamics of Wind Turbines (2nd Edition)*, Earthscan Publications Ltd, 2008.
- [13] Encyclopædie Britannica, Inc., "Turbulent Flow," 2020. [Online]. Available: <https://academic.eb.com/levels/collegiate/article/turbulent-flow/73821>. [Accessed 05 February 2020].
- [14] Encyclopædia Britannica, Inc., "Laminar Flow," 2020. [Online]. Available: <https://academic.eb.com/levels/collegiate/article/laminar-flow/46965#>. [Accessed 05 February 2020].
- [15] Y. A. Cengel and J. M. Cimbala, "Fluid mechanics: Fundamentals and applications (4th edition)," McGraw-Hill Education, 2018, p. 353 and 563.
- [16] C. E. Dole, J. E. Badick, J. R. Johnson and B. A. Johnson, "Flight Theory and Aerodynamics - A Practical Guide for Operational Safety (3rd Edition)," John Wiley & Sons., 2017.
- [17] J. Gundlach, "Designing Unmanned Aircraft Systems - A Comprehensive Approach," American Institute of Aeronautics and Astronautics, 2012.

- [18 M. P. Sforza, "Commercial Airplane Design Principles," Elsevier, 2014.
- [19 Airfoil Tools, "NACA0012 Airfoils," [Online]. Available: <http://airfoiltools.com/airfoil/details?airfoil=n0012-il>. [Accessed 15 03 2020].
- [20 Airfoil Tools, "Xfoil," [Online]. Available: <http://airfoiltools.com/airfoil/details?r=polar/index/#xfoil>. [Accessed 15 03 2020].
- [21 A. Genes, "Simple Flying," 09 September 2019. [Online]. Available: <https://simpleflying.com/aircraft-wing-tips/>. [Accessed February 2020].
- [22 Aviation Partners, "New York Times," 23 October 2013. [Online]. Available: <https://archive.nytimes.com/www.nytimes.com/interactive/2013/10/24/business/Why-Winglets.html>. [Accessed februar 2020].
- [23 R.Eppler, "Aerospace Science and Technology," Institut A fiir Mechanik, Universitiit Stuttgart, Stuttgart, 1997.
- [24 NASA Federal Agency, "Glenn Research senter," [Online]. Available: <https://www.grc.nasa.gov/www/k-12/airplane/winglets.html>. [Accessed Februar 2020].
- [25 The Boeing Company, "Boeing," [Online]. Available: http://www.boeing.com/commercial/aeromagazine/aero_17/winglet_story.html. [Accessed February 2020].
- [26 J. N. Sørensen, "General Momentum Theory for Horizontal Axis Wind Turbines," Springer, Cham, 2016, pp. 9-42.
- [27 T. Burton, N. Jenkins, D. Sharpe and E. Bossanyi, "Wind Energy Handbook (2nd Edition)," Wiley & Sons., 2011.
- [28 F. Moens and P. Gardarein, "Numerical simulation of the propeller/wing interactions for transport aircraft," *American Institute of Aeronautics & Astronautics*, 22 August 2012.
- [29 L. R. Miranda and J. E. Brennan, "Aerodynamic effects of wingtip-mounted propellers and turbines," Lockheed-California Company, San Diego, 1986.
- [30 P. Regtien and E. Dertien, "Sensors for Mechatronics (2nd Edition)," Elsevier, 2018.
- [31 Airfoil tools, "NACA 0012 AIRFOILS," [Online]. Available: <https://windeurope.org/wp-content/uploads/files/policy/position-papers/Floating-offshore-wind-energy-a-policy-blueprint-for-Europe.pdf>. [Accessed 21 May 2020].
- [32 M. Carbonaro, *Measurement Techniques Lecture Series*, von Karman Institute for Fluid Dynamics, 2014.
- [33 E. S. Abdelghany, E. E. Khalil, O. E. Abdellatif and G. elhariry, "Verizona online publishing," 08 March 2016. [Online]. Available: <http://verizonaonlinepublishing.com/ROBOTICSPDF/JournalofRoboticsandMechanicalEngineeringResearch14.pdf>. [Accessed 21 May 2020].
- [34 K. Takenaka, K. Hatanaka, W. Yamazaki and K. Nakahashi, "Multidisciplinary Design Exploration for a Winglet," *JOURNAL OF AIRCRAFT*, 2008.
- [35 J. Weierman and J. D. Jacob, "Winglet Design and Optimization for UAVs," Applied Aerodynamic Conference, Chicago, 2010.

[36 Engineering ToolBox, "Water - Dynamic and Kinematic Viscosity," 2004. [Online]. Available: https://www.engineeringtoolbox.com/water-dynamic-kinematic-viscosity-d_596.html. [Accessed 21 May 2020].

[37 Airfoil tools, "Reynolds number calculator," [Online]. Available: https://www.engineeringtoolbox.com/water-dynamic-kinematic-viscosity-d_596.html. [Accessed 21 May 2020].

[38 S. P. Neill and M. R. Hashemi, "Fundamentals of Ocean Renewable Energy," Elsevier, 2018, pp. 157-191.

8. Table of figures

Figure 1-1, Manta Wind ABs prototype..... 2

Figure 1-2, NACA0012 prototype hydrofoil..... 2

Figure 2-1. Savonius-Rotor [5] 3

Figure 2-2. Experimental Department of energy (DOE) and US Department of Agriculture (USDA) 34-meter diameter Darriues Wind turbine [7] 4

Figure 2-3, H-rotor design [7] 5

Figure 2-4, How a Fluid flows around a hydrofoil..... 6

Figure 2-5, Schematic view of streamlines past a hydrofoil 8

Figure 2-6, Definition of lift and drag 9

Figure 2-7. Boundary layer composition..... 10

Figure 2-8. Boundary layer velocity profile 10

Figure 2-9. NACA0012 profile 11

Figure 2-10, Different graphs of a NACA0012 hydrofoil. Re number ranging between 200.00 and 500.000 12

Figure 2-11, Inspiration behind a winglet comes from nature 12

Figure 2-12, Winglet Design on a glider plane 12

Figure 2-13, How the winglet affects the airstream 13

Figure 2-14. Actuator disc..... 14

Figure 2-15, Rotating flow behind a turbine VS the flow behind an actuator disc 16

Figure 2-16, Concept hydrofoil that are to be tested..... 16

Figure 3-1, Tow-tank at Western Norway University of Applied Sciences..... 19

Figure 3-2, The load cells used in this experiment is made to measure forces as high as 10kg..... 20

Figure 3-3 Basic design of a strain gauge 20

Figure 3-4, Wingtip A, B and C is all used in the experiment 23

Figure 3-5, The load cell configuration can measure forces in horizontal and vertical direction 24

Figure 3-6, The load cell is mounted on the drag-wagon with the hydrofoil connected underneath 24

Figure 3-7, Test matrix 25

Figure 3-8, Hydrofoil parts, showing the wing, different types of winglets and the drag disc 26

Figure 3-9, Calibrating the load cells before and after assembly, using weights 26

Figure 3-10, The load cell is mounted onto the tow-wagon, and the prototype onto the load cell 27

Figure 3-11, The tow-wagon moves across the pool and inflicting forces upon the hydrofoil 27

Figure 5-1, Total lift-force on the full-scale Manta Wind turbine for different velocities, the yellow stippled-line showing start-up-speed..... 32

Figure 5-2, Total Drag-force on the full-scale Manta Wind turbine for different velocities, the yellow stippled-line showing start-up-speed..... 33

Figure 5-3, Lift-to-drag ratios on the full-scale Manta Wind turbine for different velocities, the yellow stippled-line showing start-up-speed..... 33

Figure 5-4, Timeseries showing the raw data recovered from a test at velocity = 1,5m/s, angle of attack = 10 degrees and with winglet A..... 35

Figure 5-5, Comparing theoretical lift-values with experimental lift-values at velocity = 1,5m/s and winglet A..... 36

Figure 5-6, Comparing theoretical drag-values with experimental drag-values at velocity = 1,5m/s and winglet A..... 36

Figure 5-7, Different types of wingtips compared for lift at different angles. Velocity at 1,5m/s 37

Figure 5-8, Different types of wingtips compared for drag at different angles. Velocity at 1,5m/s..... 38

Figure 5-9, Lift-to-drag ratio for different wingtips at velocity at 1,5m/s..... 38

Figure 5-10, Comparing what the effect of Reynolds number has to say for the lift coefficient. Winglet type A 39

Figure 5-11, Comparing what the effect of Reynolds number has to say for the drag coefficient. Winglet type A 39

Figure 5-12, Comparing the effect of a disc-wing interaction for drag-forces at velocity = 1,5m/s and winglet A..... 40

Figure 5-13, Comparing the effect of a disc-wing interaction for lift-forces at velocity = 1,5m/s and winglet A..... 40

9. Table of Equations

Equation 1, Lift Coefficient.....	7
Equation 2, Drag Coefficient.....	7
Equation 3, Mass flow velocity	15
Equation 4, Ratio between inertia and gravity forces.....	17
Equation 5, Froude number	17
Equation 6, Equality in Reynolds number.....	18
Equation 7, Drag	21
Equation 8, Lift	21
Equation 9, Reynolds number	21
Equation 10, Areal.....	21
Equation 11, Calibration curve.....	22
Equation 12, Reynolds number	28
Equation 13, Tip-speed-ratio	30
Equation 14, Start-up velocity for the hydrofoil	30
Equation 15, Lift-to-drag ratio	31

10. Table of tables

Table 1, Scaling table	17
Table 2, An excerpt from appendix 2, showing theoretical calculations for wind velocity at 3,5 m/s and angle of attack at 10 degrees. Showing the different sections of the wing, where section 1 is the wingtip and section 6 is in the center by the hub.....	34
Table 3, Showing median chord length needed to lift the turbine into "flight-mode" at different angle of attacks and wind velocity at 3,5m/s.....	34

Attachments

Attachment 1

- Calculation NACA0012

Attachment 2

- Theoretical method - Analytical model of hydrofoil assembly

Attachment 3

- Test matrix

Attachment 4

- u15_a0-15_A - Disc interaction, timeseries and theoretical vs experimental values

Attachment 5

- Comparisson_u15

Attachment 6

- Effect of Reynolds number_Winglet A

Attachment 7

- u15_winglet C_processed data

Attachment 8

- u15_winglet B_Processed data

Attachment 9

- u15_testwithdisc_processed data

